

Physiological sharp wave-ripples and interictal events in vitro: What's the difference?

Mária R. Karlócai¹, Zsolt Kohus^{1,5}, Szabolcs Káli¹, István Ulbert^{2,3}, Gábor Szabó⁴, Zoltán Máté⁴, Tamás F. Freund¹, Attila I. Gulyás¹

¹ Laboratory of Cerebral Cortex, Institute of Experimental Medicine, Hungarian Academy of Sciences, Budapest, Hungary,

² Institute of Psychology, Hungarian Academy of Sciences, Budapest, Hungary

³ Faculty of Information Technology, Péter Pázmány Catholic University, Budapest, Hungary

⁴ Laboratory of Molecular Biology and Genetics, Institute of Experimental Medicine, Hungarian Academy of Sciences, Budapest, Hungary

⁵ Janos Szentagothai PhD Program of Semmelweis University, Budapest. Hungary

Correspondence to: Attila Gulyás

Institute of Experimental Medicine,

Hungarian Academy of Sciences

Szigony utca 43, H-1083 Budapest, Hungary

E-mail: gulyas@koki.hu

Total number of words: 7394

Summary

Sharp wave-ripples and interictal events are physiological and pathological forms of transient high activity in the hippocampus with similar features. Sharp wave-ripples have been shown to be essential in memory consolidation, while epileptiform (interictal) events are thought to be damaging. It is essential to grasp the difference between physiological sharp wave-ripples and pathological interictal events in order to understand the failure of control mechanisms in the latter case. We investigated the dynamics of activity generated intrinsically in the CA3 region of the mouse hippocampus *in vitro*, using four different types of intervention to induce epileptiform activity. As a result, sharp wave-ripples spontaneously occurring in CA3 disappeared, and following an asynchronous transitory phase, activity reorganized into a new form of pathological synchrony. During epileptiform events, all neurons increased their firing rate compared to sharp wave-ripples. Different cell types showed complementary firing: parvalbumin-positive basket cells and some axo-axonic cells stopped firing due to a depolarization block at the climax of the events in **high potassium, 4-aminopyridine and zero magnesium models, but not in the gabazine model**. In contrast, pyramidal cells started firing maximally at this stage. To understand the underlying mechanism we measured changes of intrinsic neuronal and transmission parameters in the high potassium model. We found that the cellular excitability increased and excitatory transmission was enhanced, whereas inhibitory transmission was compromised. We observed a strong short-term depression in parvalbumin-positive basket cell to pyramidal cell transmission. Thus, the collapse of pyramidal cell perisomatic inhibition appears to be a crucial factor in the emergence of epileptiform events.

Keywords: inhibitory cells, epilepsy, depolarization block, sharp wave-ripples, synchronous events

Abbreviations: 4-AP: 4-aminopyridine, aCSF = artificial cerebrospinal fluid; AP= action potential; AP5= 2R-amino-5-phosphonovaleric acid; CA = cornu Ammonis; CCK = Cholecystokinin; DG = dentate gyrus; EE = epileptiform events; GABA = gamma-aminobutyric acid; HFO = High frequency oscillation; IIE = interictal events; NBQX = 2,3-dihydroxy-6-nitro-7-sulfamoyl-benzo[f]quinoxaline-2,3-dione; NMDA = *N*-methyl-D-aspartate; PVBC = parvalbumin-positive basket cells; s.lm.= stratum lacunosum-molaculare; s.l.=

stratum lucidum; s.o.= stratum orines; s.p.= stratum pyramidale; s.r.= stratum radiatum; str = stratum; SWR = Sharp wave-ripples

Introduction

Brain states are characterized by behaviour-associated coordinated alternation of distinct EEG patterns in different cortical regions (Sirota *et al.*, 2003, Buzsaki, 2006, Isomura *et al.*, 2006). For instance, cortical slow oscillations are the result of the alternation of low activity down states and high activity up states (Steriade *et al.*, 1993, Steriade *et al.*, 1993, Steriade, 2001). A similar alternation of activity can be observed in the hippocampus during cycles of theta-embedded gamma oscillations (Soltesz and Deschenes, 1993, Bragin *et al.*, 1995) and during physiological sharp wave-ripples (SWRs, (Buzsaki, 1986, Ylinen *et al.*, 1995). This suggests that the generation of recurring transient high activity (and therefore synchronous) events is an inherent and general property of healthy cortical networks. Physiological SWRs (that are different from pathological transient events observed in epileptic patients often referred to as sharp-waves by clinicians) can be considered to be their most simple manifestation in the hippocampus, and were shown to be important in memory consolidation (Girardeau *et al.*, 2009, Jadhav *et al.*, 2012). In the epileptic hippocampus, different pathological forms of transient high activity events, including interictal (IIE), pre-ictal or ictal events (referred to as epileptic events, EEs) can be observed and are considered damaging (Engel, 1996, Aldenkamp *et al.*, 2005, Holmes and Lenck-Santini, 2006, Zhou *et al.*, 2007).

Hippocampal slices can produce spontaneously-emerging in vivo-like SWRs (Kubota *et al.*, 2003, Ellender *et al.*, 2010), while EEs can be induced upon pharmacological intervention [e.g. increasing excitability with high K^+ (Moody *et al.*, 1974, Traynelis and Dingledine, 1988), applying 4-AP (Rutecki *et al.*, 1987, Louvel *et al.*, 1994), decreasing or eliminating inhibition (Schwartzkroin and Prince, 1977, Traub and Wong, 1983, Hablitz, 1984, Miles *et al.*, 1984, Miles *et al.*, 1988) or omitting Mg^{2+} (Mody *et al.*, 1987, Jones and Heinemann, 1988, Dreier and Heinemann, 1991)]. As previously observed, the firing patterns of different hippocampal neurons were found to be modified during EEs. Most neurons increased their firing frequency, but some cells became silent, likely due to a depolarization block during the pathological events (Kawaguchi, 2001, Bikson *et al.*, 2003, Ziburkus *et al.*, 2006, Cammarota *et al.*, 2013).

In the present study, our aim was to clarify some basic differences among physiological and pathological transient high activity events. Since *in vitro* hippocampal slices can generate several different forms of transient high activity events, including both SWRs and IIEs, we induced transitions from SWRs to IIEs by different epileptiform activity-inducing treatments in order to answer the following questions: 1) What is the phenomenological difference between physiological SWRs and pathological IIEs? 2) How do the same identified neurons behave during SWRs and IIEs? 3) What are the underlying mechanisms resulting in the transition from the physiological to the pathological network state?

We found numerous differences in basic cellular and network parameters when comparing SWRs and IIEs (primarily the collapse of PVBC-mediated inhibition in the EE-producing state). These changes lead to a reorganization of synchrony and neuronal firing patterns, and result in physiological SWRs being replaced by IIEs.

Experimental procedures

Animals were kept and used according to the regulations of the European Community's Council Directive of 24 November 1986 (86/609/EEC). Experimental procedures were reviewed and approved by the Animal Welfare Committee of the Institute of Experimental Medicine, Hungarian Academy of Sciences, Budapest.

CD1 and Bl6 mice of both sexes (postnatal day 19-40) were used in the experiments. To measure selectively from cells containing the Ca²⁺ binding protein parvalbumin (PV), transgenic mice expressing enhanced green fluorescent protein (eGFP) controlled by the PV promoter were also used in this study (Meyer *et al.*, 2002). CCK (cholecystokinin) -expressing interneurons were sampled in slices prepared from CCK DsRed transgenic mice (**Table S1** and **Fig. S1**, for experimental details of the characterization of this mouse strain see *Supplemental Experimental Procedures*), where the expression of red fluorescent protein was under the control of the CCK promoter. In all cases, the mice were decapitated under deep isoflurane anaesthesia. The brain was removed into ice cold cutting solution, which had been bubbled with 95% O₂-5% CO₂ (carbogen gas) for at least 30 minutes before use. For contents of solutions see Table 1. Horizontal hippocampal slices

of 200 or 450 μm thickness were cut using a vibratome (Leica VT1000S or VT1200S), and slices were placed into an interface-type holding chamber for recovery. This chamber contained standard aCSF (**Table 1**) saturated with carbogen at 35°C that gradually cooled to room temperature. After incubation for at least 90 minutes, slices were transferred individually into a submerged-style recording chamber equipped with a dual superfusion system (Hajos *et al.*, 2009) where slices were placed on a metal mesh and two separate fluid inlets allowed aCSF to flow both above and below the slices at a rate of 3-3.5 ml/min for each flow channel, at 32-34 °C.

Standard patch electrodes were used in all recording configurations (i.e. in whole-cell patch-clamp, loose-patch and field potential recordings). Pipette resistances were 3-6 M Ω when filled with the intrapipette solution (**Table 1**) or with aCSF.

Field recordings and neuronal firing:

Data were recorded with a Multiclamp 700B amplifier (Molecular Devices, Sunnyvale, CA). Local field potentials were monitored in stratum pyramidale of the CA3 area using aCSF-filled patch pipettes. For the recording of cell firing, individual neurons in CA3 were concomitantly recorded in loose-patch mode for about 20-35 minutes. Neurons were identified visually using differential interference contrast microscopy (Olympus BX61W). Then, the pipette was withdrawn and whole-cell patch-clamp recordings were performed on the same cells with another pipette filled with intrapipette solution 1 (for contents see Table 1). Access resistance was in the range of 5-20 M Ω . Only recordings where the access resistance did not change more than 25% during the recording were included in the study. Postsynaptic potentials (PSPs) and action potentials were recorded in current clamp mode, by de- and hyperpolarizing cells to different membrane potentials (from -70mV to -30mV, 5 mV each step). The depolarization was carried out by applying a maintained current injection for 1.5-2 minutes for each step. The resting membrane potential was recorded immediately after break-in. Both field and unit recordings were low-pass filtered at 2 kHz using the built-in Bessel filter of the amplifier. Data were digitized at 6 kHz with a PCI-6042E board (National Instruments, Austin, Texas) using EVAN 1.3 software (courtesy of Prof. Istvan Mody, UCLA, CA), and were analyzed offline with custom-made programs written in MATLAB 7.0.4 and Delphi 6.0 by AIG.

Multichannel local field potential recordings

The local field potential (concomitantly at different sites) was recorded with a laminar multielectrode array placed on the surface of the hippocampal slice, parallel to the orientation of pyramidal cell dendrites spanning all hippocampal layers (24 channels, 50 μm inter-contact distance, Neuronelektrod Kft., Hungary). We used a custom-made referential amplifier system (pass-band 0.1 Hz to 7 kHz) (Ulbert *et al.*, 2001, Ulbert *et al.*, 2004). Signals were digitized with a 16 bit resolution analog-to-digital converter (National Instruments, Austin TX, USA) and recorded at 20 kHz sampling rate on each channel using a custom-made virtual instrument in LabView (National Instruments, Austin TX, USA). Current source density (CSD) calculations were made using the three-point formula smoothed by Hamming window (Ulbert *et al.*, 2001). Results are depicted by heat maps using custom-made software.

Stimulation-evoked postsynaptic currents

To record stimulation-evoked currents, 200 μm thick slices were used to minimize spontaneous network activity. Evoked inhibitory postsynaptic currents (IPSC) and excitatory postsynaptic currents (EPSC) were recorded in pyramidal cells at a holding potential of -70 mV. A stimulating electrode made of theta glass was placed into stratum radiatum to activate Schaffer collaterals or inhibitory fibres, or into the border of strata pyramidale and lucidum to evoke inhibition with a perisomatic origin. To record IPSCs and EPSCs, intrapipette solutions 2 and 3 were used, respectively (**Table 1**). When recording IPSCs, the aCSF contained 10 μM NBQX and 50 μM AP5 to block fast excitatory transmission; when EPSCs were recorded, the borders of CA3a-b and CA3b-c were cut to decrease the network size and minimize network activity. Data were digitized at 6 kHz with a PCI-6042E board (National instruments, Austin, Texas) using Stimulog software (courtesy of Prof. Zoltan Nusser, IEM, Budapest), and were analyzed off-line using the Evan software.

Inhibitory synaptic transmission

For **paired** recordings, we used 200 μm thick slices to examine changes in perisomatic inhibition (in aCSF with normal- versus high K^+). For the presynaptic cell, intrapipette solution 3 was used; the postsynaptic cell was recorded with intrapipette solution 2. The aCSF contained 10 μM NBQX and 50 μM AP5 to block fast excitatory transmission and exclude epileptic events that would interfere with the measurement of transmission. Presynaptic interneurons were held in current clamp mode around a membrane potential of -50 mV, and stimulated by a train of 30 action potentials at 150 Hz followed by 4 action potentials at 300 Hz (similar to the firing pattern recorded in loose-patch mode), 2.5–3.5 nA. Pyramidal cells were clamped at a holding potential of -50 mV (to mimic the depolarized state in elevated K^+). Series resistance was frequently monitored; cells for which the series resistance changed > 25% during recording were discarded from further analysis.

Statistics

Throughout the manuscript we applied non-parametric tests since data usually did not show a normal distribution. Thus, we used the notation nnnn (nnn; nnn) to indicate median and interquartile range. Statistical tests used were the following: Wilcoxon **paired** test, Mann-Whitney U-test, Kruskal-Wallis ANOVA, Friedman ANOVA, Kolmogorov-Smirnov test.

Further information on data analysis is available as *Supplemental Information*.

Results

Sharp wave-ripple-generating states can be switched into epileptiform event-generating states using four different epileptogenic treatments

Physiological SWRs are spontaneously generated in 450 μm thick mouse (P20-P40) hippocampal slices in aCSF (Hajos *et al.*, 2009) with features matching SWRs recorded *in vivo* (see *Supplementary Results* and **Fig. S2**). With four different epileptogenic treatments: high K^+ [8.5 mM, n=86], 4-AP [30 μM , n=8], 0 Mg^{2+} (n=19) or Gabazine [2 μM , n=23], we could evoked transitions from the SWR-generating state

to epileptiform activity-generating states (**Fig. 1**). As shown in **Fig. 1A**, the elevation of extracellular K^+ gradually eliminated SWRs and evoked a state characterized by a featureless EEG (transitory phase), followed by a state with recurring epileptiform events (**Fig. 1**) defined as large amplitude interictal-like events (IIEs) accompanied by high multi-unit activity. Both SWRs and IIEs could be recorded in hippocampal CA3 minislices in high K^+ after cutting off the dentate gyrus and area CA1, indicating that the CA3 region on its own can generate these two types of network activities (n=4, not shown).

Interictal-like events were observed in the other three models as well (**Fig. 1B**). In all four models, a transitory state that separated SWRs and IIEs appeared, with similar properties among models (**Fig. S3**). The duration of transition varied greatly among experiments within and between models. The shortest time necessary (from adding the pharmacological agent until the first EE) was 58 s (high K^+ model), whereas the longest was 2218 s in the 0 Mg^{2+} model; the median time and interquartile range (for the four models together) was 538 s (313; 560), n=136. We observed a complex reorganization of multiunit activity during the transitory state in all models. Following the transitory phase the activity evolved into IIEs, and in certain models into more complex epileptic forms (for a more detailed description of the 3 models see *Supplemental Results* and **Fig. S3**).

After demonstrating that we can successfully induce SWR-to-IIE transitions in four different ways, we focused our experiments to uncover the details of the transition in order to identify the accompanying changes in parameters and processes, with the aim of revealing the underlying mechanisms.

Sharp wave-ripples and interictal events are different transient high activity events in the high K^+ model

Analysing the occurrence of SWRs and IIEs in a large set of slices, we found that most slices producing large amplitude SWRs produced either small amplitude IIEs or no epileptic events at all. Conversely, slices with small, infrequently-emerging SWRs or no SWRs were more likely to generate epileptic events, present as large amplitude IIEs, indicating that the capability of a slice to generate either SWRs or IIEs is likely to be inversely related. To support this finding, the amplitude of SWRs and IIEs was

quantified (see *Supplemental Experimental Procedures*). Regression analysis showed a significant negative correlation between the amplitude/presence of these events (**Fig. 1C**, $p=0.013$, $R=0.48$, $n=26$).

In cases when slices did produce SWRs under control conditions and IIEs in high K^+ , the two event types never appeared interleaved. Therefore, we quantified how SWRs are replaced by IIEs ($n=25$) (**Fig. 1D**). The two types of oscillations excluded each other and were always separated by the transitory phase, strengthening the notion that they represent different network phenomena (median duration of this transitory phase was 315 sec with an interquartile range between 170 and 459 sec).

Because IIEs (especially early ones, **Fig. 1F**) could easily be mistaken for SWRs (**Fig. 1E**) we quantified the dissimilarities: First, there is a significant difference in the amplitude of the two event types; 135 μV (124.9; 141.1) for SWRs and 344 μV (299; 402) for early IIEs (Mann-Whitney U-test, $p=0.039$, differences were studied thoroughly in 10 slices). Second, SWRs and early IIEs can be separated based on their duration: SWRs lasted 46 ms (42.2; 57.4), whereas early IIEs lasted 104 ms (89.0; 115) (Mann-Whitney U-test, $p=0.026$, $n=26$). In addition, a significant difference was found in the underlying multi-unit activity: it was 170 Hz (150; 190) for SWRs and 275 Hz (160; 282) for IIEs (compared within experiments, Mann-Whitney U-test, $p<0.001$).

Early IIEs evolved into late IIEs that are more persistent events, and will therefore be examined in more detail in the present study (IIE shall refer to late IIEs from now on). We also compared their amplitude, duration and other features to those of SWRs (for SWR values see previous paragraph). A significant difference was found in the amplitude and duration of the two event types; IIE amplitude was 640 μV (512; 692) (Mann-Whitney U-test, $p=0.014$), duration was 129 ms (104; 157) (Mann-Whitney U-test, $p=0.008$, $n=26$). The third difference we found was that the period separating events from each other was 637 ms (338; 813) for SWRs and 1112 ms (862; 1794) for IIEs (Mann-Whitney U-test, $p=0.02$). Finally, a significant difference was found in the underlying multi-unit activity: it was 170 Hz (150; 190) for SWRs compared to 305 Hz (233; 466) for IIEs respectively (compared within experiments, Mann-Whitney U-test, $p<0.001$).

Differences have been described in the high-frequency component of SWRs vs. IIEs (Bragin *et al.*, 2002, Foffani *et al.*, 2007, Engel *et al.*, 2009, Levesque *et al.*, 2011), but we could not find a systematic

difference in the frequency of this component of the two types of events (using wavelet transformation), although oscillations during the peak of IIEs tended to be of slightly higher frequency and less regular than the ripples of SWRs (not shown). Current source density (CSD) analysis of the events did not demonstrate a significantly different picture either, although for the IIEs the initial source was spreading into stratum oriens and there were altered long-lasting sinks (red) and sources (blue) (**Fig. 1E, F**) in the later phase, similar to what was found in epileptic human tissue (Ulbert *et al.*, 2004, Wittner *et al.*, 2009).

After describing basic differences between the two events, we analysed the transitory phase to understand how network synchrony becomes disorganized and rearranges later into a new form of transient high activity events.

Rearrangement of synchrony during the transitory phase separates sharp wave-ripples from interictal events

Multi-unit activity during SWRs and IIEs was organized into robust, transient synchronous bursts. However, during the transitory phase leading from SWRs to IIEs the multi-unit activity gradually became asynchronous, and only after a certain time did it rearrange into a new form of synchrony (IIEs, **Fig. 2 A,B**), presumably when the level of population firing activity and its synchrony reached a threshold level (de la Prida *et al.*, 2006) and recovery dynamics after the previous event started to dominate (Staley *et al.*, 2001).

The time-binned autocorrelogram of multi-unit firing (**Fig. 2D**) displays how the clustered firing of SWRs had dissolved during the transitory phase and regrouped into another synchrony during the IIEs. To quantify and visualize the loss of synchrony leading to the transitory phase and gain of synchrony preceding IIEs, the instantaneous frequency of multi-unit activity was normalized to its low-pass filtered average. This measure clearly shows how often the firing exceeds baseline activity during the synchronous bursts. Thus the disruption and rearrangement of activity became visible (**Fig. 2C**). The local minima and maxima of the multi-unit firing frequency showed large differences during SWRs and IIEs (**Fig. 2C**), but approached each other during the transition period, suggesting a steady, elevated but less structured activity instead of high synchronies interspersed with silent periods. We also calculated the “burstiness” of multi-unit activity (see *Supplemental Experimental Procedures*), which showed a similar U-shaped curve (**Fig. 2E**). As a simple

measure of fluctuation we plotted the standard deviation of the local field potential or the multi-unit instantaneous frequency. We found that during SWRs the standard deviation values are relatively high and stable, during the transitory phase they drop and then eventually build up again to reach values higher than during SWRs (**Fig. 2F, G**). It is important to note that synchronization of multi-unit activity starts to increase long before (in the experiment shown, 2-3 minutes before) the field potential fluctuation associated with IIEs appears (period indicated with a box in **Fig. 2F**), indicating once more that an increase in multi-unit activity leads the reorganization of network activity, and gross changes in the local field potential only appear later.

So far we have described the phenomenological and behavioural differences of the hippocampal CA3 area during SWRs, the transition phase and IIEs, and have defined certain features differentiating them from one another. However, to understand the mechanisms responsible for transition we need to clarify the effects of high K^+ application on cellular and network features and parameters.

Classification of the recorded CA3 neurons

To uncover the spiking behaviour of distinct neuron types in CA3 during IIEs, we recorded local field potentials simultaneously with action potentials in loose-patch mode in neurons under visual guidance, and subsequently postsynaptic potentials (and action potentials) in whole-cell mode, followed by anatomical identification of neurons. Based on the dendritic and axonal arborisation, recorded neurons were grouped into five anatomical types: pyramidal cells (PC), parvalbumin-containing basket (PVBC) and axo-axonic cells (AAC), cholecystokinin-expressing basket cells (CCK+BC) and a mixed group of dendritic layer innervating cells (DC) (Freund and Buzsaki, 1996, Klausberger and Somogyi, 2008). The firing properties of these groups in relation to IIEs were compared (**Fig.3**). For detailed morphological descriptions see the *Supplemental Results* and **Fig. S4**.

Activity of identified cell types is different during physiological and pathological transient high activity events

We examined the firing behaviour of identified CA3 hippocampal interneurons and pyramidal cells during the transition in the high K^+ model. First we examined early IIEs. All neuron types increased their firing rate, and some showed decreased spike amplitude (**Fig.3B**). However, this altered firing pattern was changed further as early IIEs evolved into late IIEs.

A noticeable difference among early and late IIEs was that the high-frequency oscillation (Boksa *et al.*) in the local field potential during the peak of the events was significantly longer during late IIEs (81.5 ms (54.38; 92.25)) than during the early ones (27.25 ms (22.5; 40.63)) (Wilcoxon paired test, $p < 0.01$). This difference can be seen in the plot of relative power in the 150-400Hz band in the traces below the local field potential on **Fig. 3B, C**.

The firing rate of all studied neurons changed during IIEs compared to SWRs (**Fig. 3A-C, 4A and Table 2**). Since the firing pattern of different neurons varied systematically during phases of a single IIE, we defined three phases where firing properties were analysed separately: 100 ms *before* the peak of the event, 100ms *during* the event (after the multi-unit peak) and 100 ms *immediately after the event* (**Fig. 3C, 4A, B**).

Almost all neurons showed a greatly increased firing rate during IIEs compared to SWRs, with the exception of PVBCs, where the maximal firing rate only slightly exceeded the firing rate during SWRs (**Fig. 4A, Table 2**). In **Table 2**, spike numbers are described during the entire event, (duration was approximately 300-400 ms). Since SWRs last roughly 100 ms, it may be more appropriate to compare spike numbers fired during SWRs to spike numbers fired during either the "before", "during" or "after" phases. In this way we could compare spike numbers fired over similar epochs.

Pyramidal cells ($n=12$) fired with low spiking probability during SWRs (usually no spikes were detected, but in a larger, recently published dataset (Hajos *et al.*, 2013) we encountered pyramidal cells firing in association with SWRs). The firing probability significantly increased during IIEs; moreover, pyramidal cells fired bursts of action potentials between IIEs. The firing rates of pyramidal cells varied significantly between different phases of the IIEs, with a significant rise during the event, followed by a

significant drop immediately after (Friedman ANOVA and post hoc Wilcoxon paired test (**Fig. 3C, 4A, Table 2**)).

PVBC (n=10) and axo-axonic cells (n=6) fired numerous action potentials during SWRs, and fired with a somewhat higher frequency 100-150 ms prior to the large negative peak of the IIE (“before”). However, when the field event reached its negative peak (“during”), most PVBC cells and axo-axonic cells dropped their firing rate, and spike amplitude decreased gradually (**Fig. 4B, C, Table 2**). In all PVBCs and one axo-axonic cell, this decrease continued until action potentials were no longer detectable (**Table 2**). After the IIE, when the local field potential amplitude was close to baseline, the firing of the cells progressively recovered, and the spike number increased. Significant changes among phases were found for PVBCs when “before”, “during” and “after” phases were compared (Friedman ANOVA and post hoc Wilcoxon paired test, **Fig. 4A-C Table 2**), but not for axo-axonic cells.

Most CCK+ basket cells (n=5) and dendritic layer innervating cells (n=15), unlike the previous cells, fired with a moderate probability during SWRs, and increased their firing rate further during IIEs (**Fig. 3A-C Table 2**). Close to the initial negative peak of IIEs, CCK+ basket cells and dendritic layer innervating cells started firing, continued to do so during the entire event, and decreased their firing rate after the event (Friedman ANOVA and Wilcoxon paired test) (**Fig. 4B, C Table 2**).

Next, we compared the normalized changes (given as %) in firing rate (between the IIE phases) among the five neuron groups, where 100% was the number of spikes produced in the “before” phase. When examining changes between the “before” and “during” phases, PVBC values were significantly smaller than those of pyramidal cells, CCK+ basket cells and dendritic layer innervating cells; axo-axonic cell values were significantly smaller than pyramidal cell values. However, no other groups showed significant differences (differences among groups were tested with Kruskal-Wallis ANOVA followed by post hoc Mann-Whitney U-test with Bonferroni correction). When firing rate changes were compared between “before” and “after”, pyramidal cell and PVBC values were significantly smaller than axo-axonic cell and dendritic layer innervating cell values, (Kruskal-Wallis ANOVA, Mann Whitney U-test, **Fig. 4C, Tables 2 and 3**).

In the next step, we studied the extracellular spike amplitude evolution. Although only PVBCs and one axo-axonic cell decreased their firing amplitude to zero, all recorded neuron types showed somewhat decreased spike amplitude in the “during” phase. When normalized amplitudes were compared among the three activity phases for each neuron group (amplitude in the “before” phase was 100%), a significant decrease was found for pyramidal cells, PVBCs, axo-axonic cells and dendritic layer innervating cells, whereas CCK+ basket cells showed significant differences only when comparing the “during” phase to the “after” phase (Wilcoxon paired test). These data suggested that all neurons received a massive depolarization, causing a decrease in their spike amplitudes; however, the severity of the decrease differed greatly among cell types (**Fig. 4C, Table 2**).

Finally, changes in normalized spike amplitudes were compared among neuron groups, where 100% was the amplitude of spikes produced in the “before” phase. The decreased spike amplitude values of PVBCs and axo-axonic cells were significantly smaller than that of CCK+ basket cells and dendritic layer innervating cells. In addition, significant differences were found between CCK+ basket cells and dendritic layer innervating cells (normalized spike amplitude was significantly smaller for dendritic layer innervating cells, Kruskal-Wallis ANOVA, Mann Whitney U-test, **Fig. 4C, Tables 2 and 3**).

Membrane potential changes of hippocampal CA3 neurons during interictal events

The decrease in extracellular spike amplitudes and the cessation of firing suggested that cells might receive a strong depolarization and some interneurons would enter into depolarization block during IIEs. To strengthen this hypothesis we recorded the activity of neurons in whole-cell current clamp mode simultaneously with local field potential recordings. The value of the resting membrane potential and depolarization during IIEs was estimated in three different ways. This redundancy was necessary since our recordings were carried out in whole-cell mode, and even the most carefully chosen intrapipette solution can alter the intracellular ion milieu, and thus the firing of a cell. First, we compared the firing pattern recorded in loose-patch mode to the action potential pattern in whole-cell mode at different membrane potentials (**Fig 5A-C**). As shown in **Fig. 5D**, the intracellularly-recorded firing matched the loose-patch-recorded firing best

when cells were held at potentials around -30 to -40 mV between IIEs using a constant injected current. When the membrane potential was recorded in I=0 mode immediately after break-in, the membrane potential between IIEs was -35.0 mV (-40.3, -30.7) for pyramidal cells (n=8), -39.7 mV (-40.2, -39.6) for PVBCs (n=5), -45.1 mV (-45.3, -43.1) for axo-axonic cells (n=3), -41.8 mV (-42.5; -40.9) for CCK+ basket cells (n=3) and -29.7 mV (-30.4 – -29.1) for dendritic layer innervating cells (n=3). We found no significant difference among cell groups ($p=0.46$, Kruskal-Wallis ANOVA), or between membrane potentials estimated with the two methods ($p=0.318$, paired sample Wilcoxon test; to enhance readability, results are summarized in **Fig. 5, Table 4**). Finally, we calculated the approximate depolarization caused by the increase of extracellular K^+ according to the Nernst equation, which resulted in a depolarization of 23 mV (calculated with 8.5 mM K^+ in the extracellular solution compared to 3.5 mM). Since the extracellular K^+ concentration likely increases transiently during IIEs (as a result of elevated firing) (Gnatkovsky *et al.*, 2008), this result may underestimate the actual depolarization, which may reach approximately 30 mV according to previous estimates (Frohlich *et al.*, 2008, Cressman *et al.*, 2009), relative to a resting potential of -64 ± 1 mV under control conditions (Spruston and Johnston, 1992). With all calculating methods, the depolarization of the membrane potential in the high K^+ solution was about +25-35 mV compared to the estimated control membrane potential in aCSF.

Even though the baseline membrane potential showed no significant difference between cell groups in high K^+ when IIEs occurred, the membrane potential further depolarized, and the magnitude of this deflection varied among neuron groups. Since the level of this depolarization may determine whether a cell enters into depolarization block or not, we compared the maximum of the low-pass-filtered (30 Hz) membrane potential that different cell types reached during IIE peaks (in several cases this was the value of spike threshold, but in other cases membrane potential increased further during spiking, see **Fig. 5B** PVBC). Pyramidal cells and PVBCs experienced the largest depolarization (for pyramidal cells -15.5 mV (-21.5; -11.9), for PVBCs -17.6 mV (-19.9; 0)). However, only the PVBC depolarization differed significantly from the depolarization of other cell types, namely from CCK+ basket cells ($p=0.037$, Mann-Whitney U-test), and dendritic layer innervating cells ($p=0.036$, Mann-Whitney U-test) (**Fig. 5E, Table 4**), indicating that the strong depolarization can be a factor responsible for the depolarization block of PVBCs. This strong

transient depolarization cannot be the result of the temporal change in K^+ concentration (due to elevated firing during the peak of IIEs) since different cell types showed different depolarization levels.

To uncover firing characteristics of distinct cell types at different depolarization levels (threshold and depolarization block threshold), neurons were recorded in current clamp mode at different membrane potentials from -70 to -30 mV (5 mV steps, **Fig. 5E**) and the number of spikes (**Table S2**) were compared between different neuron types and different potentials. We found that when pyramidal cells, CCK+ basket cells and dendritic layer innervating cells were held around -70 mV, they fired with a low firing probability compared to what we recorded in loose-patch mode (around -40- -45 mV). For all three cell types, their firing probability was lowest at -70 mV. However, as we gradually depolarized these cells, the spiking frequency increased during IIEs (**Fig. 5E**). Conversely, in the case of PVBCs and axo-axonic cells, the firing frequency was quite high at -70 mV and gradually decreased as the cells were depolarized (lowest at -30 for PVBCs and -40 for axo-axonic cells). When the depolarization of PVBCs reached approximately -45 mV, they decreased their firing, and entered into depolarization block during IIEs, similarly to loose-patch recordings.

Firing pattern of pyramidal cells and PV+ basket cells during interictal events in other models

Since depolarization block seemed to be an important event in the generation of IIEs, we examined how the two key cell types, pyramidal cells and PVBCs, fire during IIEs in the other three models (**Fig. 6**). We found that both cell types, similar to their behaviour in high K^+ , strongly increased their firing frequency during IIEs. In the 4-AP and 0 Mg^{2+} models, PVBCs first increased their firing frequency and then entered into depolarization block around the peak of the IIE. While PVBCs were inactive, HFO appeared in the local field potential and pyramidal cells fired. In the gabazine model, although the firing did not stop at this stage, the amplitude of the spikes dropped temporarily, suggesting strong intracellular depolarization. Pyramidal cell firing again coincided here with the HFO period of the local field potential.

Since in the previous set of experiments we proved that progressive drop in extracellular action potential amplitude is the result of depolarization block of firing due to strong intracellular depolarization,

we did not make systematic experiments for the other three models. Nevertheless, we measured the membrane potential in some cells and found that, in agreement with the findings of the cell-attached recordings, cells are strongly depolarized in the 4-AP (resting membrane potential (RMP) -35 ± 7.1 mV, $n=2$ for PVBC cells, RMP: -39 ± 6.5 mV, $n=3$ for pyramidal cells) and 0 Mg^{2+} models (RMP: -40 ± 4 mV, $n=3$ for PVBC cells, RMP: -54 ± 5.9 mV, $n=3$ for pyramidal cells) but not in the gabazine model (RMP: -55 ± 8.7 mV, $n=3$ for PVBC, RMP: -53 ± 2.7 mV, $n=2$ for pyramidal cells).

Firing recorded in loose-patch mode (in all models) and intracellular potentials (examined in detail only in the high K^+ model) correlated closely with phases of the epileptic field potential. Notably, we observed interaction among firing of different cell types. Therefore, we investigated in detail the correlation between the field signal and the relative timing of the firing of different cell types.

Stages of an epileptic event correlate with intracellular potentials

Analysing local field potential features recorded simultaneously with intracellular potentials of pyramidal cells and interneurons with no injected current ($I=0$) in the high K^+ model, we found four characteristic phases of IIE evolution (**Fig. 7**):

-During the first phase, a mild negative deflection of the local field potential was associated with a small depolarization of pyramidal cells and a significant depolarization and firing frequency increase in the PVBCs, accompanied by an increase in multi-unit activity (Prida and Sanchez-Andres, 1999, de la Prida *et al.*, 2006).

-In the second phase, a steep negative shift visible on the local field potential was associated with a more pronounced pyramidal cell depolarization, and a steep depolarization of PVBCs accompanied by accelerated firing and drop in action potential amplitude. The multi-unit activity increased further.

-The onset of the third phase was defined by the blockade of PVBC firing and by a simultaneous strong depolarization of pyramidal cells associated with multiple action potentials (Trevelyan *et al.*, 2006). The HFO (see also **Fig 3 B** and **C**) that appears in this phase is most probably the population spike of the

active pyramidal cells. By the end of the phase, after an initial increase, the multi-unit activity and the pyramidal cell firing started to drop.

-During the fourth phase, the local field potential slowly returned to baseline through a negative period, the firing of PVBCs gradually recovered, pyramidal cells became repolarized to a baseline membrane potential, and stopped at a certain level of repolarization. At the same time the multi-unit activity returned to baseline (**Fig. 7**).

These phases could be distinguished in the field and cell-attached recordings of the early and late high K^+ -induced IIEs (compare **Fig. 3 B** and **C**), as well as in the other 3 models. It was the relative length and strength of the phases that were different in the early vs. late IIEs.

As we have shown above, the firing pattern of neurons becomes altered during the states that generate epileptiform activity. This can be the result of either changes in cellular parameters important in signal integration, or alterations in the parameters of excitatory and inhibitory transmission. In the next steps we set out to reveal the possible basis of the observed alterations.

High K^+ application alters cellular and network parameters

First we measured basic parameters of pyramidal cells ($n=9$) in high K^+ and compared them to control conditions. As shown in **Fig. 8A** we found that the membrane potential of cells depolarized from -59.2 mV (-62.1; -56.4) to -35.5 mV (-41.2; -27.1), their input resistance decreased from 68.2 MOhm (42.1; 114.8) to 29.1 MOhm (28.8; 44.2), and the threshold of the current injection required to induce at least one action potential (during a step protocol with 800 ms long de- and hyperpolarising steps) decreased from 177 pA (153; 213) to 37 pA (-156; 124).

Next we measured the effect of high K^+ on excitatory and inhibitory transmission. In pyramidal cells we recorded inhibitory postsynaptic currents (IPSCs) evoked with local electric stimulation at the border of strata pyramidale and lucidum (to measure changes in perisomatic inhibition), or in stratum radiatum (to estimate the alteration in dendritic inhibition). In both cases we found a significant decrease in IPSC amplitude to 45% of control (29.4; 54.9) for perisomatic inhibition ($p=0.004$ paired Wilcoxon test, **Fig. 8B**)

and to 58.5% of control (36.2; 78.9) for dendritic inhibition ($p=0.002$ paired Wilcoxon test, **Fig. 8C**). Then excitatory postsynaptic potentials (EPSCs) evoked in stratum radiatum were recorded in pyramidal cells. When K^+ was elevated, we found a significant increase in EPSC amplitude to 132.6% of control (92.3; 216.1) ($p=0.002$, paired Wilcoxon test, **Fig. 8D and E**).

The question arose if altered action potential shape (amplitude and/or width, charge transfer) can be responsible for the changes in excitatory and inhibitory transmission. We examined how these parameters changed during high K^+ wash in (for more details see *Supplemental Results*). Since in both inhibitory cells and in pyramidal cells we saw similar changes (**Fig. S6**), this cannot be a mechanism responsible for the simultaneous increase of excitatory transmission and decrease of inhibitory transmission.

These data indicate that the efficiency of synaptic inhibition is decreased, whereas excitatory synaptic transmission is increased in high K^+ . We observed the strongest depression in perisomatic inhibition, which is considered to be the most important in the control of pyramidal cell firing (Cobb *et al.*, 1995, Miles *et al.*, 1996). Therefore, we carried out paired recordings of monosynaptically coupled perisomatic inhibitory-pyramidal cell pairs (PVBC-pyramidal cell, axo-axonic cell-pyramidal cell and CCK+ basket cell-pyramidal cell) to uncover the exact changes affecting the transmitter release of different perisomatic interneurons.

The strength and short-term depression of PV-containing basket cells inhibitory action is modulated by high K^+ application.

Presynaptic cells were targeted in slices prepared from transgenic mice expressing fluorescent markers in PV- or CCK-containing neurons. Postsynaptic currents were evoked by a train of action potentials triggered in the presynaptic cell, similar to the firing of these cells recorded during IIEs (30 APs with 150 Hz followed by 4 action potentials with 300 Hz). We compared the peak amplitudes and inhibitory charges recorded in pyramidal cells in control conditions and in elevated K^+ (probably due to plastic processes in high K^+ , washout did not typically result in a complete reversal of the effects of treatment (see **Fig. 8D**)). IPSCs in pyramidal cells evoked by PVBCs ($n=7$) and axo-axonic cells ($n=7$) significantly

decreased in amplitude in high K^+ . However, IPSCs in pyramidal cells evoked by CCK+ basket cells (n=5) remained fairly intact (for IPSC peak amplitudes: p=0.03 for PVBC-pyramidal cell pairs, p=0.03 for axo-axonic cell-pyramidal cell pairs and p=0.44 for CCK+ basket cell-pyramidal cell pairs; for inhibitory charge: p=0.03 for PVBC-pyramidal cell pairs, p=0.03 for axo-axonic cell-pyramidal cell pairs and p=0.625 for CCK+ basket cell-pyramidal cell pairs, paired Wilcoxon tests; to enhance readability, results are summarised in **Fig. 8F and Table 4**). We also found that both during control conditions and in high K^+ the IPSCs often disappeared before the train ended during the train from PVBCs and axo-axonic cells, indicating that neurotransmission cannot be sustained at the high frequency of firing throughout IIEs. In contrast, a sustained transmission and asynchronous release was found (Hefft and Jonas, 2005, Szabo *et al.*, 2010) (Szabo *et al.*, 2010) in case of CCK+ basket cells, even in the presence of high K^+ .

Our final question was whether short-term depression becomes altered in high K^+ . Therefore, the amplitude of the first 10 IPSCs was compared to the amplitude of the first IPSC (Pn/P1), illustrated in **Fig. 8H**. In the case of PVBCs (n=7), short term depression became more pronounced in high K^+ (grey) for the first 10 peaks compared to control conditions (black, p<0.01, Kolmogorov-Smirnov), whereas no such change appeared in the case of axo-axonic cells (n= 7, p=0.42, Kolmogorov-Smirnov). In contrast, when IPSCs originating from CCK+ basket cells (n=5) were studied in high K^+ , the depression was less pronounced. Moreover, plasticity could transiently switch from depression to facilitation (p<0.01, Kolmogorov-Smirnov, **Fig. 8G**).

Thus, perisomatic inhibition provided by PV+ interneurons becomes largely ineffective during an epileptic event, whereas the inhibitory transmission of CCK+ basket cells remains fairly intact or occasionally, even slightly increased.

Discussion

In the present study we wished to describe the difference between physiological SWRs and IIEs.

Unfortunately, the term sharp wave-ripple used by neurobiologists for physiological events is misleading for neurologists/clinicians who use the term “sharp wave” to identify an EEG element occurring in association

with epilepsy. This term was borrowed by the biologist from the clinical EEG nomenclature, but it identifies a healthy pattern essential in learning and memory formation.

We have shown that: 1) *in vitro* SWRs and IIEs are indeed different network phenomena with distinct properties. Upon pharmacological interference SWRs disappear and, following a transitory phase, the network activity reorganises into a new form of activity in all examined models. 2) During IIEs all CA3 neurons fire with increased firing rate compared to SWRs. However, the firing of PVBCs and some axo-axonic cells stop (except for the gabazine model) due to depolarization block before the climax of the event. 3) During IIEs the firing of PVBCs and pyramidal cells are complementary; i.e., pyramidal cells start firing when PVBCs get into depolarization block, while dendritic inhibitory cells fire strongly during all phases of the IIEs. 4) In high K^+ the balance of excitation to inhibition is shifted: inhibitory transmission is compromised, excitation is enhanced, and the integrative properties of pyramidal cells also change, resulting in higher excitability. 5) Inhibition collapses for several synergistic reasons: first, as PVBCs and axo-axonic cells enter into depolarization block, they stop firing action potentials; second, even when action potentials are generated, GABA release is greatly decreased (this is true for all recorded inhibitory cells, but mainly for PVBCs and axo-axonic cells); and, finally, the short-term depression of IPSCs originating from PVBCs is increased in high K^+ .

Physiological sharp wave-ripples and interictal events are distinct types of transient high activity events

Though the field potential signal of SWRs and IIEs recorded in stratum pyramidale may look similar in shape, they differ in several features (amplitude, duration, accompanying multi-unit activity, firing pattern of neurons). As opposed to SWRs, during IIEs all pyramidal cells are repetitively active. We proved that IIEs never evolve from SWRs but are separated by a featureless transitory phase, where coordinated firing characteristic of SWRs is disrupted, the baseline activity (multi-unit activity) increases and disorganised firing evolves.

Highly active low synchrony states similar to the one observed during the transition phase were found in other *in vitro* epilepsy models induced by decreasing GABAergic inhibition (Cohen *et al.*, 2006, de la Prida *et al.*, 2006), adding 4-AP (Perreault and Avoli, 1991, Barbarosie and Avoli, 1997), omitting Mg^{2+} (Whittington *et al.*, 1995, Huberfeld *et al.*, 2011), or decreasing Ca^{2+} (Bikson *et al.*, 2003), strengthening the hypothesis that SWRs and IEs represent different types of network activity. However, this activity did not persist as a stable network state. When the population activity reached a critical level, a new type of synchrony, IEs, (as well as at later stages IEs of different complexity) appeared in our slices, similar to results published earlier (Khosravani *et al.*, 2005). The results of the theoretical paper by Brunel and Wang (Brunel and Wang, 2003) might explain why the two types of transient synchrony are mutually exclusive, as well as the presence of the unstructured gap between them. They explored the effect of changing excitatory and inhibitory transmission parameters, showing that network dynamics could be pushed from one type of oscillation to a mechanistically different one with an unorganised/asynchronous state in between. They reasoned that there are parameter ranges where the network cannot generate a synchronous state, since the proper timing of recurrent feed-back mechanisms is not ensured.

Inhibitory control, especially from PV+BCs, fails during interictal events for several reasons

At the beginning of an IE the spontaneous firing of highly excitable pyramidal cells may reach a level of run-away excitation (Lux and Heinemann, 1978, Frohlich *et al.*, 2008) and the build-up of excitation in the initiating pyramidal cell population is manifested as the first step of depolarization both in inhibitory neurons and pyramidal cells (Fig. 8). Although in our set of pyramidal cells we could hardly see any spiking in association with SWRs, in a recently published, larger dataset we did see a subset of pyramidal cells firing before and during SWRs (Hajos *et al.*, 2013). Furthermore, as shown on Fig. S5 and Figs. 5 and 7 phase 1&2, intracellular recordings reveal that SWRs and IEs are preceded by a build-up of depolarizing potentials, indicating increasing excitatory neuron activity.

In parallel with the increase in excitation, inhibitory neuron populations start to be activated. There is a level of excitation, however, when PVBCs and some axo-axonic cells enter into depolarization block (in most models), and the build-up of excitation enters an uncontrolled state where all pyramidal cells (relieved

from perisomatic inhibition) fire repetitively. In the 0 Mg²⁺ model it has previously been shown that pyramidal cells do activate, and IIEs can propagate with a larger speed when inhibition is terminated (Trevelyan *et al.*, 2006, Trevelyan *et al.*, 2007).

Similar inactivation (depolarization block) of fast-spiking cells has previously been described in cortical slices using the 0 Mg²⁺ or the 4-AP model (Kawaguchi 2001, Cammarota 2013). The validity of our finding is further supported by recent clinical findings in epileptic patients showing that inhibitory cells enter into depolarization block at the beginning of seizures (Omar J. Ahmed, Wilson Truccolo, Jacob A. Donoghue, Emad N. Eskandar, G. Rees Cosgrove, N. Stevenson Potter, Andrew S. Blum, Leigh R. Hochberg, Sydney S. Cash; Human inhibitory single neurons switch off before dramatic increases in seizure intensity, AES Meeting, San Diego, 2012). In addition, recent animal studies have shown that decreasing the activity of pyramidal cells, could delay electrographic and behavioural initiation of status epilepticus (Sukhotinsky *et al.*, 2013) or decrease paroxysmal activity in cell culture (Tonnesen *et al.*, 2009). Besides inhibiting pyramidal cells, activating PV-containing cells can also reduce seizure frequency of epilepsy (Krook-Magnuson *et al.*, 2013), indicating that restoring the activity of PVBCs could effectively decrease pyramidal cell firing and control network activity. It is a future task however, to build a clinical approach aiming to normalize the firing of strategically crucial neuron types.

Why is inhibitory control sufficient during SWRs, whereas it fails during IIEs? It seems that inhibition is compromised in the high K⁺ state at three stages: 1) there is a general decrease of inhibitory transmission strength even for single action potentials, especially for perisomatic inhibition (**Fig 8B and C**), 2) the transmission of PV⁺ cells, characterized by multiple high-frequency spiking during an EE suffers a strong (for PVBCs an almost complete) short-term depression (**Fig 8G**) and 3) the most effective inhibitory neurons, PVBCs, enter into depolarization block before the peak of IIEs (**Figs 3, 4 and 5**). Although dendritic inhibitory neurons and CCK⁺ basket cells keep firing with increasing frequency and their transmission is potentiated somewhat, it seems that they cannot control the runaway firing of pyramidal cells during IIEs (they actually might even promote pyramidal cell firing by reducing their entry into depolarization block, see below).

Features of PV+ basket cells that make them vulnerable to excess excitation

The next question is why PVBCs and some axo-axonic cells get into depolarization block while other interneurons and pyramidal cells escape. Depolarization block of neurons was observed in pioneering *in vivo* studies of neocortical and hippocampal seizures using intracellular recordings from single unidentified cells (Kandel and Spencer, 1961, Matsumoto and Marsan, 1964). The involvement of Na⁺ channels and persistent sodium current has been shown to be critical in the evolution of depolarization block (Bikson *et al.*, 2003). The transition from sustained spiking to depolarization block can be described using dynamical systems theory (Izhikevich, 2007, Dovzhenok and Kuznetsov, 2012). Although no detailed mathematical analysis of the relationship between cellular parameters and the input current required for depolarization block has been performed, the conditions leading to depolarization block likely depend on the properties (such as the voltage-dependence and kinetics of channel activation and inactivation) and densities of spike-generating currents, but may also be influenced by slower (e.g., adaptation) currents. The properties of both Na⁺ and K⁺ channels are known to be different in PVBCs and pyramidal cells (Martina and Jonas, 1997, Martina *et al.*, 1998). Another important factor which determines whether depolarization block occurs is the net input current (synaptic current) received by the neuron, which may differ substantially among the different cell types. In fact, we showed here that during IIEs, PVBCs and axo-axonic cells reach more depolarized membrane potentials compared to other cell types. This can be explained by the fact that PV+ cells receive significantly more excitatory (~15,000) inputs, balanced with a weak inhibition (6%) compared to CCK+ (~5000 excitatory input, 35% inhibition) and dendritic inhibitory neurons (~2600 excitatory input, 29% inhibition (Gulyas *et al.*, 1999, Matyas *et al.*, 2004). **On the other hand, pyramidal cells have a dendritic input organization that is rather similar to that of PV+ cells.** They receive a large amount of excitatory input (~30,000 synapses) that is balanced only by a weak inhibition (5.3%, (Megias *et al.*, 2001)); still, they do not get into depolarization block during IIEs. One of the reasons for this is probably the observed differences in spike-generating current as discussed above; another important difference may be the presence of slower adaptation currents (such as M-type and sAHP K⁺ currents) in pyramidal cells, but not in PVBCs. **Most importantly, the perisomatic input organization of the two cell types is different. While PVBCs do receive**

perisomatic and somatic excitatory inputs, pyramidal cells are devoid of them, and therefore might not experience the same depolarization block as PVBCs do (Gulyas *et al.*, 1999, Megias *et al.* 2001). It has been shown that in neurons not receiving perisomatic excitation, the soma and the axon are electrotonically distant (Rancz and Hausser, 2010), and therefore might not experience the same depolarization as neurons with perisomatic excitatory input. Thus, a unique combination of cellular and connectivity parameters in PVBCs may act synergistically to explain the presence of depolarization block during IIEs. As a result, the enhanced excitation effectively activates pyramidal cells without causing a depolarization block, and without PVBC-mediated control over spiking, the network activity further increases.

Spike time histograms showed that except for PVBCs, all neuron types could considerably increase their firing rate during IIEs compared to SWRs. An important implication of our results is that PVBCs, by receiving a large amount of excitatory input and expressing the proper combination of ion channels, are tuned to be able to fire maximally during physiological, transient, high activity events, i.e., the SWRs. On the other hand, a detrimental consequence of this fine tuning is that when they receive a pathologically high level of excitation, they enter into depolarization block – i.e. the fuse blows.

Absolute and relative changes in cellular and network properties underlie the switch from healthy to pathological synchrony in the high K^+ model

Combining the results of Brunel and Wang with our findings (long-term changes of cellular and network parameters and transient changes in inhibitory transmission, firing patterns of different cell types) as well as with earlier results demonstrating that pyramidal cells and interneurons become activated at different times during IIEs (Trevelyan *et al.*, 2006, Ziburkus *et al.*, 2006, Spampanato and Mody, 2007), we suggest the following sequence of events during the evolution of IIEs:

1) **Initiation stage:** Deflections in the local field potential, increasing spiking of neurons (multi-units and cell-attached spikes) as well as two-phased depolarization of intracellular potentials suggest that excitatory activity starts to build up gradually at the beginning of an IIE (phase 1 and 2 of **Fig. 7**), similar to the case of SWRs (Hajos *et al.*, 2013). However, since the strength and the balance of excitatory and inhibitory transmission, as well as cellular excitability, is shifted by high K^+ application (compared to

SWRs), although inhibition is still present in this phase, it can not restrain the excitation from building-up further in the recurrent system of CA3.

2) Pyramidal cell firing/HFO stage: As the activity in the system increases beyond the physiological level, inhibition totally fails (phase 3) through different synergistic mechanisms (depolarization block of PVBCs, short term depression of IPSCs) and most pyramidal cells start to fire at high frequency. These high frequency, synchronized action potentials are manifested as HFO in the local field potential (Dzhala and Staley, 2004, Foffani *et al.*, 2007). It is important to note that since perisomatic inhibitory transmission has collapsed at this point, synchronous IPSPs do not contribute to local field potential generation in stratum pyramidale, unlike in the case of the generation of the ripples of SWRs (Csicsvari *et al.*, 1999, Klausberger *et al.*, 2003, Le Van Quyen *et al.*, 2008, Hajos *et al.*, 2013).

3) Termination stage: Examining phase 4 in Fig. 7 might give a clue as to why IIEs terminate. Here we can see that pyramidal cell firing accommodates and starts to slow down, while PVBCs are still in depolarization block (the same is visible in the drop of multi-unit frequency for all models in Fig. 1B). So it is the refractoriness of the pyramidal cells that is the first step in the termination. As pyramidal cells fire less, inhibition regains control and terminates the IIE. Paradoxically, the depolarization block of PVBCs (evidently a refractory mechanism) can help terminate IIEs, since while the cells are not firing their inhibitory transmission might recover from the strong depression, and when the cells start firing again their inhibition is effective. The decreasing firing frequency of PVBCs in phase 4 (**Fig.7**) indicates that their excitatory drive decreases (note that before they stop firing due to depolarization block their firing frequency keeps increasing, so they do not slow due to accommodation, but due to decreasing drive). Most probably several refractory mechanisms are engaged by the end of phase 3 due to the repetitive high frequency firing of the pyramidal cells. Collapse of glutamatergic transmission or refractoriness of the firing might be elements that result in decreased pyramidal cell firing and the recovery of inhibition.

Isomorphic mechanisms might lead to IIEs in different models and play a role in the generation of more complex EEs

We measured in detail how cellular and network parameters change in the high K^+ model. We found that the excitability of neurons, as well as the absolute and relative values of excitatory and inhibitory

transmission, become altered. Other employed epilepsy-inducing treatments also evoke changes in these critical parameters. 4-AP application causes a blockade of voltage-gated K^+ channels (Glover, 1982, Rudy, 1988, Choquet and Korn, 1992), and thus changes input resistance and membrane potential. Zero Mg^{2+} activates NMDA receptors and induces an increase in excitatory transmission, leading to direct depolarization (Flatman *et al.*, 1983, Coan and Collingridge, 1985, Mody *et al.*, 1987) and long term potentiation of synaptic transmission (Kauer *et al.*, 1988). Gabazine directly increases excitability by blocking synaptic and non-synaptic $GABA_A$ receptors, thus eliminating inhibition and depolarizing cells (Heulme *et al.*, 1987, Aradi and Maccaferri, 2004, Wlodarczyk *et al.*, 2013), as well as by increasing input resistance (Cope *et al.*, 2005). Recent work by Aivar and Prida (personal communication) also demonstrates changes in the strength and ratio of excitatory and inhibitory transmission in an *in vitro* epileptic model induced by low Ca^{2+} concentration.

The findings of Brunel and Wang (2003), especially in the light of their later study (Geisler *et al.*, 2005), leaves enough room for possible parameter changes to push the system into different dynamics. The work of Marder (Marder, 2011) also emphasizes that in the case of neurons and networks, several different sets of parameter combinations can result in similar or identical behaviours. Recent results of genetic studies revealed that epilepsies with similar symptomatology can be caused by highly distinct mutations in different genes (Poduri and Lowenstein, 2011, Allen *et al.*, 2013).

These ideas drove us to suggest a common framework for all the studied models: As a first step, shifts of different nature in excitability, and a change in the ratio of excitation vs. inhibition, are induced in the different epilepsy induction models, resulting in a pathological, uncontrolled increase of activity during the initiation phase of IIEs.

As a second step, inhibition fails during the pyramidal cell firing/HFO stage in all but the gabazine model. After the activity builds up to a sufficiently high level, excitatory drive makes PVBCs fire at a non-physiologically high frequency, resulting in strong short term depression of inhibitory transmission that releases pyramidal cells from inhibition, which then start firing at high frequency, generating the HFO in the local field potential. Inhibition is further damaged because PVBCs enter into an additional depolarization

block that evolves because elevated K^+ , 4-AP and zero Mg^{2+} causes direct strong depolarization of the membrane that is further boosted by the strong excitation during the initiation stage.

PVBCs do not enter depolarization block in the gabazine model, probably because although gabazine causes some depolarization by inhibiting synaptic and non-synaptic $GABA_A$ currents (Cope *et al.*, 2005), this depolarization may not be enough to push the membrane into depolarization block. Yet, the pyramidal cell firing/HFO stage is present in this model too. We believe that the initiation stage starts due to compromised inhibition (so the lack of PVBC depolarization block is irrelevant), and at some stage the uncontrolled build-up of excitation causes masses of pyramidal cells to reach the threshold for high frequency firing, and the IIE enters the pyramidal cell firing/HFO stage.

In these models, the last step, the termination stage of IIEs, is possibly driven by the same refractory mechanisms in the excitatory system as in the high K^+ model, since we see a similar drop in pyramidal cell firing by the end of the second stage.

To explain all stages of the IIEs, we invoked two layers of parameter changes on different time scales. The prolonged parameter modulation, the difference between the healthy and the epileptic state, manifests on the several-minute time-scale of epileptiform activity induction. In epileptic patients this is probably the original reason why epilepsy starts: later events are consequences. The alteration of parameters means that IIEs are initiated instead of SWRs. As a second layer, short term changes (collapse of inhibition, refractoriness of excitation on the 200-1000msec scale of an IIE) allow uncontrolled firing and later termination of a single cycle. If we want to explain the evolution of EE forms (early and late interictal, preictal and ictal), we have to invoke a third layer of changes that is a superimposed slow drift in the parameters (on the 1-5 minute scale), most probably evoked by pathologically high activity (changes in K^+ levels, metabolic exhaustion, potentiation of synaptic weights, etc). This drift results in changes in the initiation rate and recurrent structure of IIE like bursts, as well as in the relative length of their different stages (e.g. HFO stage is longer during late IIEs than during early IIEs). We propose that preictal and ictal events are combinations of repetitive, degenerated IIEs. There must be a secondary refractory mechanism

associated with the third layer as well, since repetitive ictal events are almost always followed by silent periods lasting for minutes.

ACKNOWLEDGEMENTS:

Prof. Péter Halász (National Institute of Neurosciences, Budapest, Hungary) and Dr. Dániel Fabó (National Institute of Neurosciences, Budapest, Hungary) kindly helped us to classify in vitro epileptiform activities.

We are grateful to those who were kind to read the manuscript: Marco de Curtis, Norbert Hájos and Richard Miles. We also thank Dr. Hannah Monyer for generously providing the PV eGFP mice. The authors thank

The authors also thank the Nikon Microscopy Center at IEM, Nikon Austria GmbH and Auro-Science Consulting Ltd for kindly providing microscopy support.

Katalin Lengyel, Erzsebet Gregori and Győző Goda for excellent technical support.

This work was supported by: Hungarian Scientific Research Fund (OTKA K83251 and OTKA 81357),

ERC-2011-ADG-294313 (SERRACO), National Office for Research and Technology NKTH-ANR,

Neurogen and Multisca, European Union Seventh Framework Program (NeuroSeke) and TÁMOP-4.2.1.B-

11/2/KMR-2011-0002

List of References

- Aldenkamp AP, Beitzler J, Arends J, van der Linden I, Diepman L. Acute effects of subclinical epileptiform EEG discharges on cognitive activation. *Funct Neurol*. 2005;20(1):23-8.
- Allen AS, Berkovic SF, Cossette P, Delanty N, Dlugos D, Eichler EE, et al. De novo mutations in epileptic encephalopathies. *Nature*. 2013;501(7466):217-21.
- Aradi I, Maccaferri G. Cell type-specific synaptic dynamics of synchronized bursting in the juvenile CA3 rat hippocampus. *The Journal of neuroscience : the official journal of the Society for Neuroscience*. 2004;24(43):9681-92.
- Barbarosie M, Avoli M. CA3-driven hippocampal-entorhinal loop controls rather than sustains in vitro limbic seizures. *J Neurosci*. 1997;17(23):9308-14.
- Bikson M, Hahn PJ, Fox JE, Jefferys JG. Depolarization block of neurons during maintenance of electrographic seizures. *J Neurophysiol*. 2003;90(4):2402-8.
- Boksa P, Wilson D, Rochford J. Responses to stress and novelty in adult rats born vaginally, by cesarean section or by cesarean section with acute anoxia. *Biol Neonate*. 1998;74(1):48-59.
- Bragin A, Jando G, Nadasdy Z, Hetke J, Wise K, Buzsaki G. Gamma (40-100 Hz) oscillation in the hippocampus of the behaving rat. *J Neurosci*. 1995;15(1 Pt 1):47-60.
- Bragin A, Mody I, Wilson CL, Engel J, Jr. Local generation of fast ripples in epileptic brain. *J Neurosci*. 2002;22(5):2012-21.
- Brunel N, Wang XJ. What determines the frequency of fast network oscillations with irregular neural discharges? I. Synaptic dynamics and excitation-inhibition balance. *Journal of neurophysiology*. 2003;90(1):415-30.
- Buzsaki G. Hippocampal sharp waves: their origin and significance. *Brain Res*. 1986;398(2):242-52.
- Buzsaki G. *Rhythms of the Brain*. New York: Oxford University Press; 2006.
- Camarota M, Losi G, Chiavegato A, Zonta M, Carmignoto G. Fast spiking interneuron control of seizure propagation in a cortical slice model of focal epilepsy. *The Journal of physiology*. 2013;591(Pt 4):807-22.
- Choquet D, Korn H. Mechanism of 4-aminopyridine action on voltage-gated potassium channels in lymphocytes. *J Gen Physiol*. 1992;99(2):217-40.
- Coan EJ, Collingridge GL. Magnesium ions block an N-methyl-D-aspartate receptor-mediated component of synaptic transmission in rat hippocampus. *Neurosci Lett*. 1985;53(1):21-6.
- Cobb SR, Buhl EH, Halasy K, Paulsen O, Somogyi P. Synchronization of neuronal activity in hippocampus by individual GABAergic interneurons. *Nature*. 1995;378(6552):75-8.
- Cohen I, Huberfeld G, Miles R. Emergence of disinhibition-induced synchrony in the CA3 region of the guinea pig hippocampus in vitro. *J Physiol*. 2006;570(Pt 3):583-94.
- Cope DW, Hughes SW, Crunelli V. GABAA receptor-mediated tonic inhibition in thalamic neurons. *The Journal of neuroscience : the official journal of the Society for Neuroscience*. 2005;25(50):11553-63.
- Cressman JR, Jr., Ullah G, Ziburkus J, Schiff SJ, Barreto E. The influence of sodium and potassium dynamics on excitability, seizures, and the stability of persistent states: I. Single neuron dynamics. *J Comput Neurosci*. 2009;26(2):159-70.

- Csicsvari J, Hirase H, Czurko A, Mamiya A, Buzsaki G. Oscillatory coupling of hippocampal pyramidal cells and interneurons in the behaving Rat. *J Neurosci*. 1999;19(1):274-87.
- de la Prida LM, Huberfeld G, Cohen I, Miles R. Threshold behavior in the initiation of hippocampal population bursts. *Neuron*. 2006;49(1):131-42.
- Dovzhenok A, Kuznetsov AS. Exploring neuronal bistability at the depolarization block. *PloS one*. 2012;7(8):e42811.
- Dreier JP, Heinemann U. Regional and time dependent variations of low Mg²⁺ induced epileptiform activity in rat temporal cortex slices. *Exp Brain Res*. 1991;87(3):581-96.
- Dzhala VI, Staley KJ. Mechanisms of fast ripples in the hippocampus. *The Journal of neuroscience*. 2004;24(40):8896-906.
- Ellender TJ, Nissen W, Colgin LL, Mann EO, Paulsen O. Priming of hippocampal population bursts by individual perisomatic-targeting interneurons. *J Neurosci*. 2010;30(17):5979-91.
- Engel J, Jr. Introduction to temporal lobe epilepsy. *Epilepsy Res*. 1996;26(1):141-50.
- Engel J, Jr., Bragin A, Staba R, Mody I. High-frequency oscillations: what is normal and what is not? *Epilepsia*. 2009;50(4):598-604.
- Flatman JA, Schwindt PC, Crill WE, Stafstrom CE. Multiple actions of N-methyl-D-aspartate on cat neocortical neurons in vitro. *Brain research*. 1983;266(1):169-73.
- Foffani G, Uzcategui YG, Gal B, Menendez de la Prida L. Reduced spike-timing reliability correlates with the emergence of fast ripples in the rat epileptic hippocampus. *Neuron*. 2007;55(6):930-41.
- Freund TF, Buzsaki G. Interneurons of the hippocampus. *Hippocampus*. 1996;6(4):347-470.
- Frohlich F, Bazhenov M, Iragui-Madoz V, Sejnowski TJ. Potassium dynamics in the epileptic cortex: new insights on an old topic. *Neuroscientist*. 2008;14(5):422-33.
- Geisler C, Brunel N, Wang XJ. Contributions of intrinsic membrane dynamics to fast network oscillations with irregular neuronal discharges. *Journal of neurophysiology*. 2005;94(6):4344-61.
- Girardeau G, Benchenane K, Wiener SI, Buzsaki G, Zugaro MB. Selective suppression of hippocampal ripples impairs spatial memory. *Nat Neurosci*. 2009;12(10):1222-3.
- Glover WE. The aminopyridines. *Gen Pharmacol*. 1982;13(4):259-85.
- Gnatkovsky V, Librizzi L, Trombin F, de Curtis M. Fast activity at seizure onset is mediated by inhibitory circuits in the entorhinal cortex in vitro. *Annals of neurology*. 2008;64(6):674-86.
- Gulyas AI, Megias M, Emri Z, Freund TF. Total number and ratio of excitatory and inhibitory synapses converging onto single interneurons of different types in the CA1 area of the rat hippocampus. *J Neurosci*. 1999;19(22):10082-97.
- Hablitz JJ. Picrotoxin-induced epileptiform activity in hippocampus: role of endogenous versus synaptic factors. *J Neurophysiol*. 1984;51(5):1011-27.
- Hajos N, Ellender TJ, Zemankovics R, Mann EO, Exley R, Cragg SJ, et al. Maintaining network activity in submerged hippocampal slices: importance of oxygen supply. *Eur J Neurosci*. 2009;29(2):319-27.

- Hajos N, Karlocai MR, Nemeth B, Ulbert I, Monyer H, Szabo G, et al. Input-output features of anatomically identified CA3 neurons during hippocampal sharp wave/ripple oscillation in vitro. *The Journal of neuroscience : the official journal of the Society for Neuroscience*. 2013;33(28):11677-91.
- Heaulme M, Chambon JP, Leyris R, Wermuth CG, Biziere K. Characterization of the binding of [3H]SR 95531, a GABAA antagonist, to rat brain membranes. *Journal of neurochemistry*. 1987;48(6):1677-86.
- Hefft S, Jonas P. Asynchronous GABA release generates long-lasting inhibition at a hippocampal interneuron-principal neuron synapse. *Nat Neurosci*. 2005;8(10):1319-28.
- Holmes GL, Lenck-Santini PP. Role of interictal epileptiform abnormalities in cognitive impairment. *Epilepsy Behav*. 2006;8(3):504-15.
- Huberfeld G, Menendez de la Prida L, Pallud J, Cohen I, Le Van Quyen M, Adam C, et al. Glutamatergic pre-ictal discharges emerge at the transition to seizure in human epilepsy. *Nat Neurosci*. 2011;14(5):627-34.
- Isomura Y, Sirota A, Ozen S, Montgomery S, Mizuseki K, Henze DA, et al. Integration and segregation of activity in entorhinal-hippocampal subregions by neocortical slow oscillations. *Neuron*. 2006;52(5):871-82.
- Izhikevich E. *Dynamical systems in neuroscience*. . Cambridge, MA: The MIT Press; 2007.
- Jadhav SP, Kemere C, German PW, Frank LM. Awake hippocampal sharp-wave ripples support spatial memory. *Science*. 2012;336(6087):1454-8.
- Jones RS, Heinemann U. Synaptic and intrinsic responses of medial entorhinal cortical cells in normal and magnesium-free medium in vitro. *J Neurophysiol*. 1988;59(5):1476-96.
- Kandel ER, Spencer WA. The pyramidal cell during hippocampal seizure. *Epilepsia*. 1961;2:63-9.
- Kauer JA, Malenka RC, Nicoll RA. NMDA application potentiates synaptic transmission in the hippocampus. *Nature*. 1988;334(6179):250-2.
- Kawaguchi Y. Distinct firing patterns of neuronal subtypes in cortical synchronized activities. *The Journal of neuroscience : the official journal of the Society for Neuroscience*. 2001;21(18):7261-72.
- Khosravani H, Pinnegar CR, Mitchell JR, Bardakjian BL, Federico P, Carlen PL. Increased high-frequency oscillations precede in vitro low-Mg seizures. *Epilepsia*. 2005;46(8):1188-97.
- Klausberger T, Magill PJ, Marton LF, Roberts JD, Cobden PM, Buzsaki G, et al. Brain-state- and cell-type-specific firing of hippocampal interneurons in vivo. *Nature*. 2003;421(6925):844-8.
- Klausberger T, Somogyi P. Neuronal diversity and temporal dynamics: the unity of hippocampal circuit operations. *Science*. 2008;321(5885):53-7.
- Krook-Magnuson E, Armstrong C, Oijala M, Soltesz I. On-demand optogenetic control of spontaneous seizures in temporal lobe epilepsy. *Nat Commun*. 2013;4:1376.
- Kubota D, Colgin LL, Casale M, Brucher FA, Lynch G. Endogenous waves in hippocampal slices. *J Neurophysiol*. 2003;89(1):81-9.
- Le Van Quyen M, Bragin A, Staba R, Crepon B, Wilson CL, Engel J, Jr. Cell type-specific firing during ripple oscillations in the hippocampal formation of humans. *The Journal of neuroscience : the official journal of the Society for Neuroscience*. 2008;28(24):6104-10.
- Levesque M, Bortel A, Gotman J, Avoli M. High-frequency (80-500 Hz) oscillations and epileptogenesis in temporal lobe epilepsy. *Neurobiol Dis*. 2011;42(3):231-41.

- Louvel J, Avoli M, Kurcewicz I, Pumain R. Extracellular free potassium during synchronous activity induced by 4-aminopyridine in the juvenile rat hippocampus. *Neurosci Lett*. 1994;167(1-2):97-100.
- Lux HD, Heinemann U. Ionic changes during experimentally induced seizure activity. *Electroencephalogr Clin Neurophysiol Suppl*. 1978(34):289-97.
- Marder E. Variability, compensation, and modulation in neurons and circuits. *Proc Natl Acad Sci U S A*. 2011;108 Suppl 3:15542-8.
- Martina M, Jonas P. Functional differences in Na⁺ channel gating between fast-spiking interneurons and principal neurons of rat hippocampus. *The Journal of physiology*. 1997;505 (Pt 3):593-603.
- Martina M, Schultz JH, Ehmke H, Monyer H, Jonas P. Functional and molecular differences between voltage-gated K⁺ channels of fast-spiking interneurons and pyramidal neurons of rat hippocampus. *The Journal of neuroscience : the official journal of the Society for Neuroscience*. 1998;18(20):8111-25.
- Matsumoto H, Marsan CA. Cortical Cellular Phenomena in Experimental Epilepsy: Ictal Manifestations. *Exp Neurol*. 1964;9:305-26.
- Matyas F, Freund TF, Gulyas AI. Convergence of excitatory and inhibitory inputs onto CCK-containing basket cells in the CA1 area of the rat hippocampus. *Eur J Neurosci*. 2004;19(5):1243-56.
- Megias M, Emri Z, Freund TF, Gulyas AI. Total number and distribution of inhibitory and excitatory synapses on hippocampal CA1 pyramidal cells. *Neuroscience*. 2001;102(3):527-40.
- Meyer AH, Katona I, Blatow M, Rozov A, Monyer H. In vivo labeling of parvalbumin-positive interneurons and analysis of electrical coupling in identified neurons. *J Neurosci*. 2002;22(16):7055-64.
- Miles R, Toth K, Gulyas AI, Hajos N, Freund TF. Differences between somatic and dendritic inhibition in the hippocampus. *Neuron*. 1996;16(4):815-23.
- Miles R, Traub RD, Wong RK. Spread of synchronous firing in longitudinal slices from the CA3 region of the hippocampus. *J Neurophysiol*. 1988;60(4):1481-96.
- Miles R, Wong RK, Traub RD. Synchronized afterdischarges in the hippocampus: contribution of local synaptic interactions. *Neuroscience*. 1984;12(4):1179-89.
- Mody I, Lambert JD, Heinemann U. Low extracellular magnesium induces epileptiform activity and spreading depression in rat hippocampal slices. *Journal of neurophysiology*. 1987;57(3):869-88.
- Moody WJ, Futamachi KJ, Prince DA. Extracellular potassium activity during epileptogenesis. *Exp Neurol*. 1974;42(2):248-63.
- Perreault P, Avoli M. Physiology and pharmacology of epileptiform activity induced by 4-aminopyridine in rat hippocampal slices. *J Neurophysiol*. 1991;65(4):771-85.
- Poduri A, Lowenstein D. Epilepsy genetics--past, present, and future. *Curr Opin Genet Dev*. 2011;21(3):325-32.
- Prida LM, Sanchez-Andres JV. Nonlinear frequency-dependent synchronization in the developing hippocampus. *J Neurophysiol*. 1999;82(1):202-8.
- Rancz EA, Hausser M. Dendritic spikes mediate negative synaptic gain control in cerebellar Purkinje cells. *Proc Natl Acad Sci U S A*. 2010;107(51):22284-9.
- Rudy B. Diversity and ubiquity of K channels. *Neuroscience*. 1988;25(3):729-49.

- Rutecki PA, Lebeda FJ, Johnston D. 4-Aminopyridine produces epileptiform activity in hippocampus and enhances synaptic excitation and inhibition. *J Neurophysiol.* 1987;57(6):1911-24.
- Schwartzkroin PA, Prince DA. Penicillin-induced epileptiform activity in the hippocampal in vitro preparation. *Ann Neurol.* 1977;1(5):463-9.
- Sirota A, Csicsvari J, Buhl D, Buzsaki G. Communication between neocortex and hippocampus during sleep in rodents. *Proc Natl Acad Sci U S A.* 2003;100(4):2065-9.
- Soltesz I, Deschenes M. Low- and high-frequency membrane potential oscillations during theta activity in CA1 and CA3 pyramidal neurons of the rat hippocampus under ketamine-xylazine anesthesia. *J Neurophysiol.* 1993;70(1):97-116.
- Spampanato J, Mody I. Spike timing of lacunosom-moleculare targeting interneurons and CA3 pyramidal cells during high-frequency network oscillations in vitro. *J Neurophysiol.* 2007;98(1):96-104.
- Spruston N, Johnston D. Perforated patch-clamp analysis of the passive membrane properties of three classes of hippocampal neurons. *J Neurophysiol.* 1992;67(3):508-29.
- Staley KJ, Bains JS, Yee A, Hellier J, Longacher JM. Statistical model relating CA3 burst probability to recovery from burst-induced depression at recurrent collateral synapses. *J Neurophysiol.* 2001;86(6):2736-47.
- Steriade M. To burst, or rather, not to burst. *Nat Neurosci.* 2001;4(7):671.
- Steriade M, Nunez A, Amzica F. Intracellular analysis of relations between the slow (< 1 Hz) neocortical oscillation and other sleep rhythms of the electroencephalogram. *J Neurosci.* 1993;13(8):3266-83.
- Steriade M, Nunez A, Amzica F. A novel slow (< 1 Hz) oscillation of neocortical neurons in vivo: depolarizing and hyperpolarizing components. *J Neurosci.* 1993;13(8):3252-65.
- Sukhotinsky I, Chan AM, Ahmed OJ, Rao VR, Gradinaru V, Ramakrishnan C, et al. Optogenetic delay of status epilepticus onset in an in vivo rodent epilepsy model. *PloS one.* 2013;8(4):e62013.
- Szabo GG, Holderith N, Gulyas AI, Freund TF, Hajos N. Distinct synaptic properties of perisomatic inhibitory cell types and their different modulation by cholinergic receptor activation in the CA3 region of the mouse hippocampus. *Eur J Neurosci.* 2010;31(12):2234-46.
- Tonnesen J, Sorensen AT, Deisseroth K, Lundberg C, Kokaia M. Optogenetic control of epileptiform activity. *Proc Natl Acad Sci U S A.* 2009;106(29):12162-7.
- Traub RD, Wong RK. Synchronized burst discharge in disinhibited hippocampal slice. II. Model of cellular mechanism. *J Neurophysiol.* 1983;49(2):459-71.
- Traynelis SF, Dingledine R. Potassium-induced spontaneous electrographic seizures in the rat hippocampal slice. *J Neurophysiol.* 1988;59(1):259-76.
- Trevelyan AJ, Sussillo D, Watson BO, Yuste R. Modular propagation of epileptiform activity: evidence for an inhibitory veto in neocortex. *The Journal of neuroscience : the official journal of the Society for Neuroscience.* 2006;26(48):12447-55.
- Trevelyan AJ, Sussillo D, Yuste R. Feedforward inhibition contributes to the control of epileptiform propagation speed. *The Journal of neuroscience : the official journal of the Society for Neuroscience.* 2007;27(13):3383-7.

Ulbert I, Halgren E, Heit G, Karmos G. Multiple microelectrode-recording system for human intracortical applications. *J Neurosci Methods*. 2001;106(1):69-79.

Ulbert I, Heit G, Madsen J, Karmos G, Halgren E. Laminar analysis of human neocortical interictal spike generation and propagation: current source density and multiunit analysis in vivo. *Epilepsia*. 2004;45 Suppl 4:48-56.

Ulbert I, Magloczky Z, Eross L, Czirjak S, Vajda J, Bognar L, et al. In vivo laminar electrophysiology co-registered with histology in the hippocampus of patients with temporal lobe epilepsy. *Exp Neurol*. 2004;187(2):310-8.

Whittington MA, Traub RD, Jefferys JG. Erosion of inhibition contributes to the progression of low magnesium bursts in rat hippocampal slices. *The Journal of physiology*. 1995;486 (Pt 3):723-34.

Wittner L, Huberfeld G, Clemenceau S, Eross L, Dezamis E, Entz L, et al. The epileptic human hippocampal cornu ammonis 2 region generates spontaneous interictal-like activity in vitro. *Brain*. 2009;132(Pt 11):3032-46.

Wlodarczyk AI, Sylantyev S, Herd MB, Kersante F, Lambert JJ, Rusakov DA, et al. GABA-independent GABAA receptor openings maintain tonic currents. *The Journal of neuroscience : the official journal of the Society for Neuroscience*. 2013;33(9):3905-14.

Ylinen A, Bragin A, Nadasdy Z, Jando G, Szabo I, Sik A, et al. Sharp wave-associated high-frequency oscillation (200 Hz) in the intact hippocampus: network and intracellular mechanisms. *J Neurosci*. 1995;15(1 Pt 1):30-46.

Zhou JL, Lenck-Santini PP, Zhao Q, Holmes GL. Effect of interictal spikes on single-cell firing patterns in the hippocampus. *Epilepsia*. 2007;48(4):720-31.

Ziburkus J, Cressman JR, Barreto E, Schiff SJ. Interneuron and pyramidal cell interplay during in vitro seizure-like events. *J Neurophysiol*. 2006;95(6):3948-54.

Table 1: Composition of extra-and intracellular solutions

Extracellular solutions											
in mM	Sucrose	NaCl	KCL	NaHCO3	CaCl2	MgCl2	NaH2PO4	glucose			
aCSF	0	126	3.5	26	1.6	1.2	1.25	10			
cutting	205	0	2.5	26	0.5	5	1.25	10			
Intracellular solutions		pH 7.39, osmolarity of 285 mOsmL									
in mM	K-gluconate	CsCl	MgCl	HEPES	NaCl	Mg-ATP	ATP	GTP	Creatine phosphate	QX-314	biocytin
Intra 1	110		0	40	4	2	0	0.3	0	0	0.20%
Intra 2	80 (Cs-gluconate)	60	1	10	3	0	2		0	5	0.20%
Intra 3	138	3	0	10	0	4	0	0.4	10	0.2	0.20%

For Peer Review

Table 2: Spiking characteristics of different hippocampal CA3 neurons during SWRs and during different phases of EEs, and values of significance when comparing them. Numbers in italics are significant p values (<0.05).

	PC	PV+ BC	AAC	CCK+ BC	DN
spike/SWR	0	2.9 (0.9;5.1)	2.1 (0.9; 2.5)	0.6 (0.2; 0.8)	0.8 (0.4; 1.8)
spike/IE	11.8 (4.7; 11.6)	6.7 (7.7; 11.5)	12.8 (7.1; 18.6)	15.1 (11.5; 14.7)	11.7 (8.9; 15.9)
Wilcoxon test p values	<0.001	0.038	0.008	0.03	<0.001

Median number of APs across events in different phases	PC	PV+ BC	AAC	CCK+ BC	DN
APs "before" phase	2.5 (2.4; 4.9)	4.5 (3.5; 8.1)	7 (3.9; 8)	4.89 (4.1; 5.8)	3.69 (3.3; 5.3)
APs "during" phase	8.5 (4; 9.3)	0.76 (0.5; 1)	4.18 (2.6; 4.7)	6.88 (1.6; 5.7)	5.13 (0.6; 1.6)
APs "after" phase	0.17 (0.1; 4.2)	1.1 (0.4; 1.5)	3.74 (3.3; 5.4)	2.5 (1.7; 3.2)	3.1 (1.5; 4.2)

change in firing rate (spike number in "before" phase: 100%)					
"before" to "during"	211 (148.5; 325%)	12.5 (7.6; 23.9%)	100.4 (58.2; 136.2%)	129 (107; 154%)	129 (33.1; 200.1%)
"before" to "after"	6.7 (3.5; 8.9%)	36.81 (14.1; 37%)	76.6 (73.7; 121.8%)	47.9 (33.3; 65.1%)	69.1 (55.5; 93%)
"during" to "after" (during was 100%)	4.3 (2.1; 7.7%)	223.4 (58.1; 421%)	89.5 (34.2; 126.6%)	41 (38.9; 46.9%)	62.9 (32.6; 99.7%)
Friedman ANOVA	<0.001	0.007	0.8	0.015	0.011
Post hoc corrected Wilcoxon test p values					

"before" to "during"	0.026	0.024	0.68	0.29	0.4
"before" to "after"	0.016	0.02	0.5	0.13	0.03
"during" to "after"	0.014	0.024	0.92	0.043	0.42

change in spike amplitude (amplitude in "before" phase: 100%)					
"before" to "during"	54.4% (66.7; 87.6)	65.3% (49.5; 75)	54.89% (54.9; 68.4)	98.5% (96.4; 103.1)	73.14% (63.9; 86.7)
"before" to "after"	78.4% (61.2; 86.3)	71.2% (61.2; 76.5)	66.94% (66.3; 76.4%)	111.6% (107;113.3%)	89.87% (77.4; 98%)
"during" to "after" (during was 100%)	109.8% (76.5; 112.6)	109.1% (102; 128.9)	125.9 % (108.9; 138.6)	106% (102.5; 117.4)	116.1% (103; 128.5)
Wilcoxon test p values					
"before" to "during"	0.009	0.005	0.043	1	0.004
"before" to "after"	0.018	0.005	0.028	0.144	0.012
"during" to "after"	0.57	0.05	0.075	0.043	0.004

Table 3: Spiking characteristics of different hippocampal CA3 neurons during SWRs and during different phases of EEs, and values of significance when comparing them. Numbers in italics are significant p values (<0.05).

Levels of significance when comparing relative changes of firing rate and amplitude among cell groups. As post hoc test, Mann-Whitney U-test is used with Bonferroni correction.

Kruskal-Wallis ANOVA: p=0.011		PC	PV+ BC	AAC	CCK+ BC
Firing rate change: before to during	PC				
	PV+BC	<i><0.001</i>			
	AAC	<i>0.046</i>	<i>0.062</i>		
	CCK+BC	<i>0.137</i>	<i>0.014</i>	<i>0.27</i>	
	DN	<i>0.084</i>	<i>0.002</i>	<i>0.35</i>	<i>0.89</i>

Kruskal-Wallis ANOVA: p=0.006		PC	PV+ BC	AAC	CCK+ BC
Firing rate change: before to after	PC				
	PV+BC	<i>0.27</i>			
	AAC	<i>0.023</i>	<i>0.023</i>		
	CCK+BC	<i>0.056</i>	<i>0.143</i>	<i>0.39</i>	
	DN	<i>0.036</i>	<i>0.018</i>	<i>0.48</i>	<i>0.35</i>

Kruskal-Wallis ANOVA: p<0.001		PC	PV+ BC	AAC	CCK+ BC
Spike amplitude change: before to during	PC				
	PV+BC	<i>0.24</i>			
	AAC	<i>0.098</i>	<i>0.85</i>		
	CCK+BC	<i>0.08</i>	<i>0.012</i>	<i>0.004</i>	
	DN	<i>0.16</i>	<i>0.043</i>	<i>0.13</i>	<i>0.028</i>

Kruskal-Wallis ANOVA: p<0.001		PC	PV+ BC	AAC	CCK+ BC
Spike amplitude change: before to after	PC				
	PV+BC	<i>0.015</i>			
	AAC	<i>0.22</i>	<i>0.7</i>		
	CCK+BC	<i>0.06</i>	<i>0.012</i>	<i>0.028</i>	
	DN	<i>0.5</i>	<i>0.008</i>	<i>0.028</i>	<i>0.038</i>

For Peer Review

Table 4: Membrane potential characteristics of different CA3 neurons during EEs.

Transmission parameters of different perisomatic-pyramidal cell pairs among different conditions.

Membrane pot. closest to loose patch pattern	PC	PV+ BC	AAC	CCK+ BC	DN
Membrane pot. I=0	-30.8 mV (-32; -30.3)	-39.7 mV (-40.2; -39.6)	-45.1 mV (-45.3; -43)	-41.8 mV (-42.5; -40.9)	-29.7 mV (-30.4; -29.1)
Membrane pot at IIE peak	-13.1mV (-15.4; -11.9)	-17.6 mV (-19.9; 0)	-19.9 mV (-20.2; -15.2)	-29.9 mV (-33.8; -29.1)	-28 mV (-29.1; -27.8)
Membrane potential where firing probability is the highest	-35.1 mV (-36.4; -33.8)	-40.4 mV (-45.1; -29.8)	-40.4 mV (-45.2; -40.2)	-44.8 mV (-45.1; -42.3)	-30.4 mV (-32.8; -30.1)

IPSG (nS) %	PV+ BC	AAC	CCK+ BC
high K+ (control: 100%)	45.3% (33.4; 49.1)	37.3% (11.2; 56.5)	73.44% (54.3; 93)
Washout	57.5% (38.4; 88.9)	61.7% (54.5; 139)	93.7% (72.2; 167.5)

amplitude (pA) %	PV+ BC	AAC	CCK+ BC
high K+ (control: 100%)	42.2% (26.3; 51.7)	65.3% (51.9; 70.4)	76.9% (73.7; 80.8)
Washout	98.3% (93; 137.8)	97.5% (88.1; 111.2)	98.9% (91.8; 106)

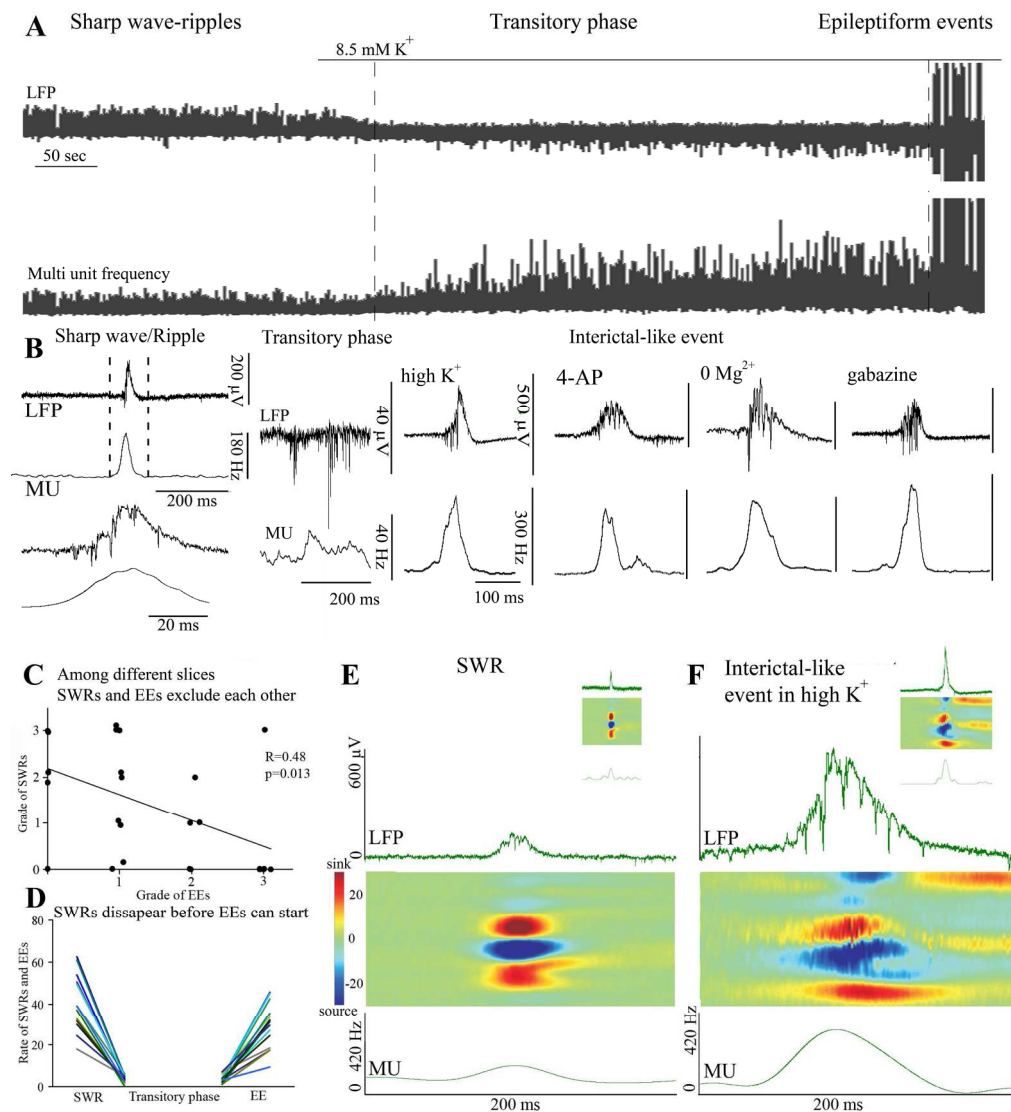


Figure 1: Transition from sharp-wave ripples to epileptiform events and their differences

A) IIEs were induced by elevating extracellular K^+ concentration. A highly active, desynchronized state separates the physiological, transiently highly active SWR state from the pathological, transiently highly active IIEs. Note that an increase of multi-unit frequency precedes IIEs. Upper traces: local field potential of the transitory phase. Lower traces: Plot of multiunit frequency demonstrating network activity during the transition. B) Enlarged image of a SWR and accompanying multi-unit activity at two time scales, as well as the transitory phase and IIEs and the underlying multi-unit activities appearing in four different epilepsy models. C) Physiological and pathological transient high activity events are plotted to compare their correlation. A negative correlation is present in the rate of amplitude of the two types of events ($n=26$). D) The rate of SWRs and IIEs at three different phases of the transition from several experiments. During control conditions SWR rate is high (and EE rate is 0), but after the pharmacological intervention it disappears completely. After the transitory phase (when the rate of both SWRs and IIEs is 0) the rate of IIEs starts to increase, whereas SWR rate remains at zero. Note that for slices able to generate both SWRs and IIEs, the IIEs cannot be seen until SWRs disappear completely ($n=25$).

SWRs (E) and early IIEs (F) may appear similar (see insets), however, compared to SWRs, IIEs (even early ones) have a larger amplitude, a longer duration (top trace) and are accompanied by several-fold higher

multi-unit activity (bottom trace). Analysis of current source densities (centre) showed only minor shifts in the organization of sinks (red) and sources (blue), especially in the second half of an event.

199x222mm (300 x 300 DPI)

For Peer Review

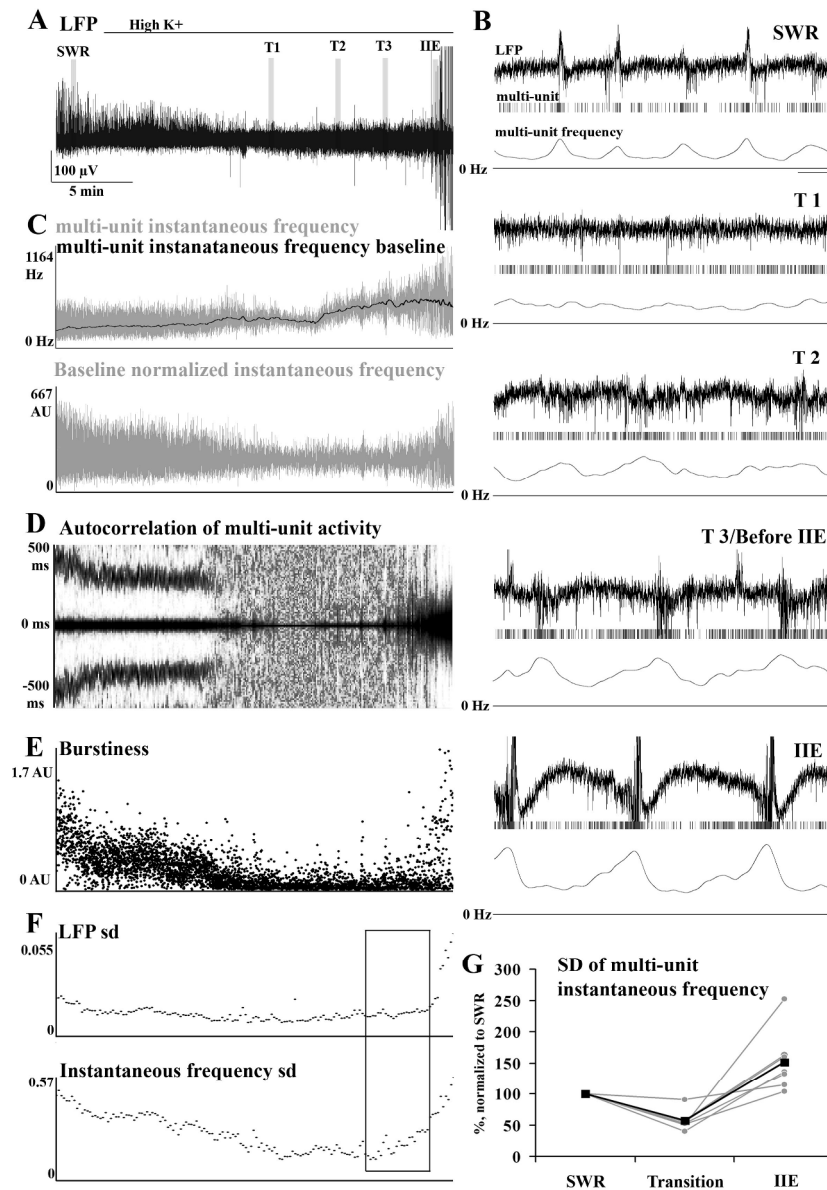


Figure 2: Reorganization of synchrony during sharp-wave ripple to epileptiform event transition induced by high K+

During the transition the synchrony of multi-unit activity drops and then builds up again until the network reaches the level of synchrony where IIEs start. A) Local field potential during the transitory phase. Areas emphasized with grey bars (SWR, T1, T2, T3 and IIE) indicate different phases of the transition and are magnified in B. The raster plot of multi-units and the multi-unit frequency are shown below the local field potential. C) Upper trace shows how multi-unit frequency (grey) and its low-pass-filtered baseline (black) increases during the transition. The lower graph shows the baseline-normalized instantaneous frequency fluctuation. D) Time-binned autocorrelogram of multi-unit activity showing that the synchrony of firing during SWRs falls apart during the transitory period and reorganizes into a different synchrony during IIEs.

E) A U-shaped curve of "burstiness" of multi-unit frequency shows that during the transition phase, synchrony decreases in the system. F) A decrease and gradual recovery can be seen both in the standard deviation (s.d.) of local field potential values and in the s.d. of instantaneous multiunit frequency. Note that

the s.d. of multi-unit frequency starts to increase several minutes earlier than the s.d. of the local field potential signal (framed area), and a high level of synchrony evolves before anything is seen in the local field potential. G) Changes in the standard deviation of multi-unit instantaneous frequency from SWRs to the transition phase and to IIEs in 6 recordings. Scale: B upper 100 μ V, lower 60 Hz, time scale: 500 ms

202x292mm (300 x 300 DPI)

For Peer Review

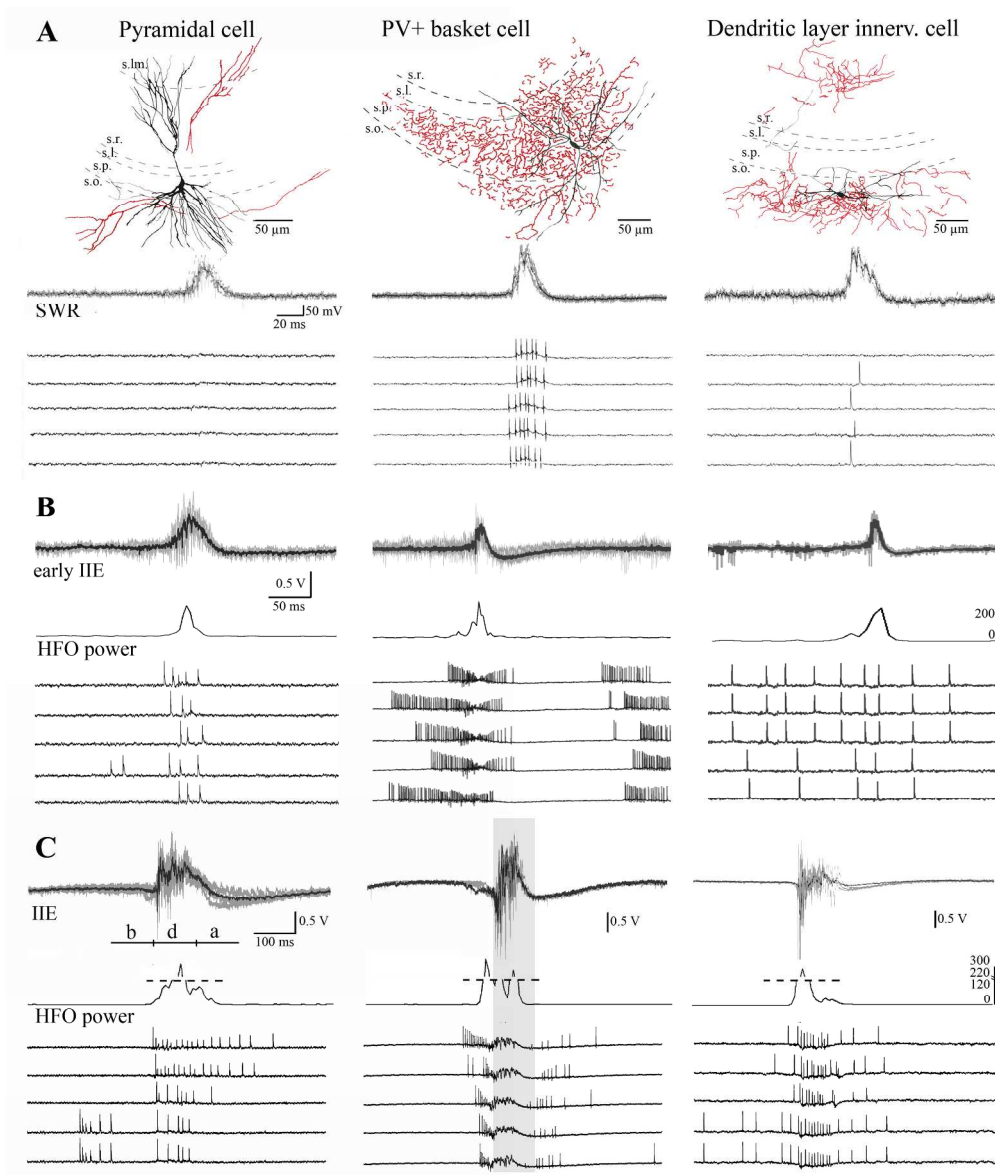


Figure 3: While parvalbumin-positive basket cells stop firing during epileptiform events, other cells increase their firing rate

A) Firing of anatomically identified CA3 neurons during SWRs recorded in loose patch mode. Somata and dendrites of cells are shown in black, axons in red. Firing of the cells can be seen in the lower rows. B-C) Firing of neurons during early and late IIEs, respectively. All examined neurons increased their firing rate and changed their firing pattern during early IIEs. During late IIEs they increased their firing rate further, and some cells (PVBCs) stopped firing at the peak. Below the local field potential the relative power in the 150-400Hz band is plotted to show the duration of high-frequency oscillation during the IIEs. HFO coincided with pyramidal cell firing and the silent phase of PVBCs. For quantification, firing of neurons was separated into three phases of 100 ms: before (b), during (d) and after (a) the peak of the IIE. PVBCs stopped firing at the peak (grey area, approximately "during" phase) of IIEs.

248x295mm (300 x 300 DPI)

For Peer Review

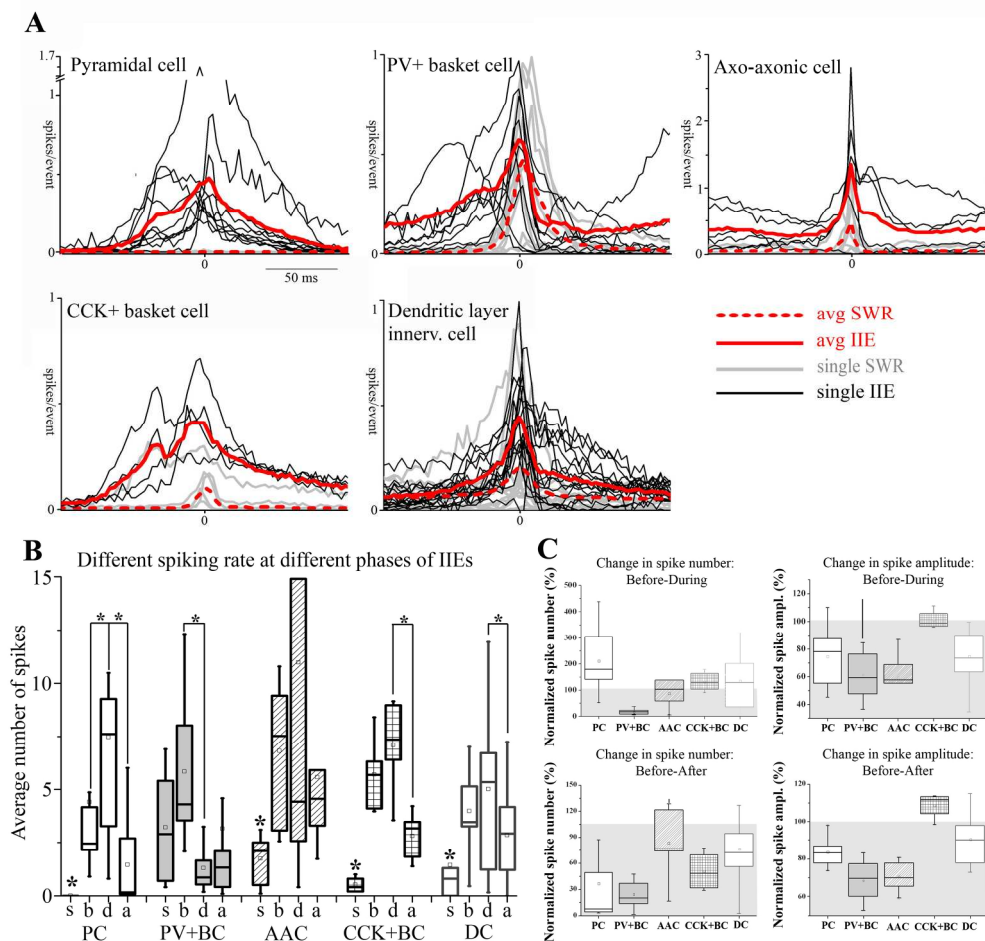


Figure 4: Firing rate varies among different phases of epileptiform events induced by high K+
 A) Spike distribution histograms of individual neurons during SWRs (grey: individual traces, dashed red: average) and IIEs (black: individual traces, red: average) show that the firing pattern becomes altered and the firing rate increases. B) Statistical comparison of the average number of spikes fired by different neurons during SWRs (s), in the "before" (b), "during" (d) and "after" (a) phases. Note that the spike number significantly increases from SWRs to IIEs (marked with asterisks). Firing also differs greatly among different phases of IIEs. C) Changes in normalized firing probability and amplitude for different neuron types (normalized to "before" phase). Upper graphs compare changes in normalized values between the "before" and the "during" phases, whereas lower traces compare changes among the "before" and "after" phases. Grey area indicates a decrease (below 100%), asterisks indicate significance at $p < 0.05$.

202x193mm (300 x 300 DPI)

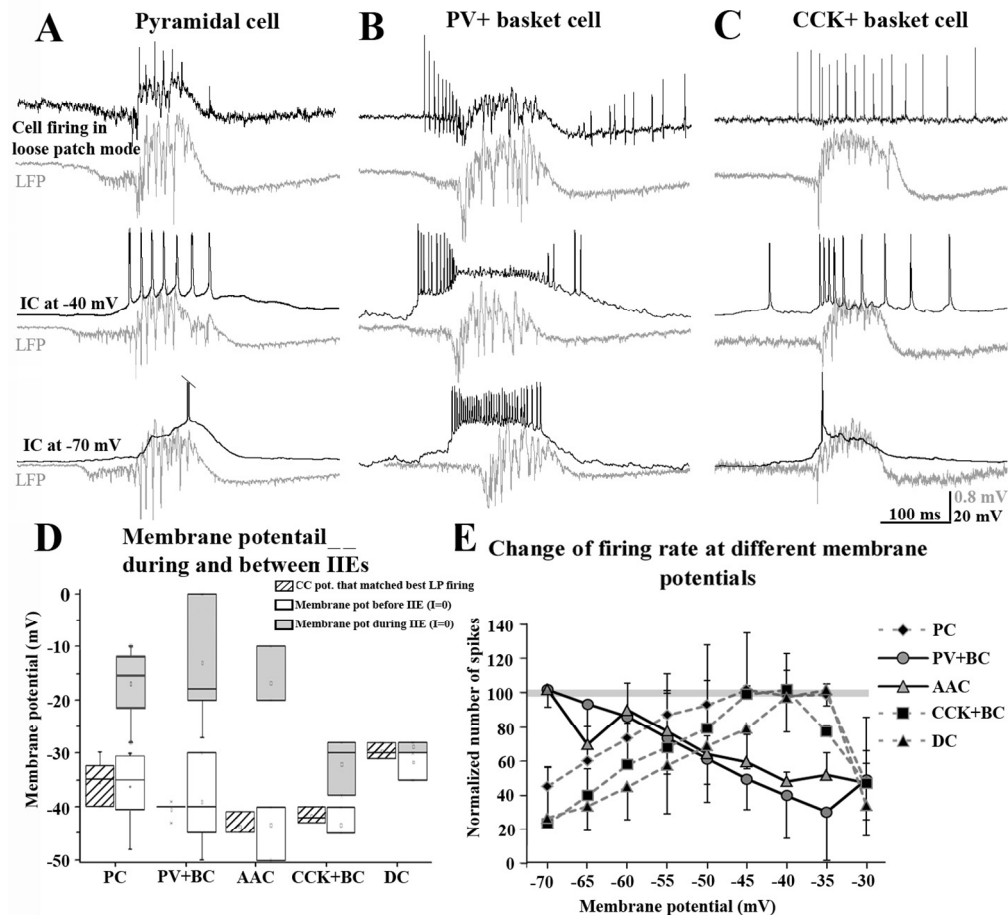


Figure 5: Parvalbumin-positive basket cell firing is blocked due to strong depolarization

A-C) Three examples show that in the epileptogenic aCSF the membrane potential of neurons is approximately -40mV before IIEs (baseline), since their loose-patch-recorded spiking matches the firing pattern recorded at -40mV in current clamp during IIEs. Upper pair of traces show loose-patch-recorded firing (black) during an IIE (grey: local field potential). Similar sequences of spikes were recorded from the neuron at -40mV (middle traces), but not at -70mV (lower traces). The similarity to the -40 mV potential was true for all examined cell types. A pyramidal cell (A), a PVBC (B) and a CCK+ basket cell (C) are shown.

D) The membrane potential where neurons fired with a similar pattern to that seen in loose patch mode is indicated with the lower striped grey box and whiskers (baseline), whereas the membrane potential recorded immediately after break-in (in $I=0$ mode) is shown with white box and whiskers. Higher grey box and whiskers indicate the membrane potential recorded during the IIE peak. This value was markedly higher compared to the former two time points, and was more variable among cells.

E) Change in spiking rate as a function of depolarization is shown for CA3 neurons. Some neurons increase their firing rate upon depolarization (pyramidal cell, CCK+ basket cell, dendritic layer innervating cell) while others decrease it (PVBC, axo-axonic cell). To compare neurons with inherently different spiking rates, membrane potential-dependent changes were normalized to the peak firing rate of individual neurons. Grey line indicates 100% as maximal firing. The figure shows that PVBCs and axo-axonic cells fire already maximally close to normal resting potential (note that PVBCs may completely stop firing, whereas, axo-axonic cells only drop their firing rate until a certain point). Other neurons, most importantly pyramidal cells, can increase their firing rate with depolarization.

120x112mm (300 x 300 DPI)

For Peer Review

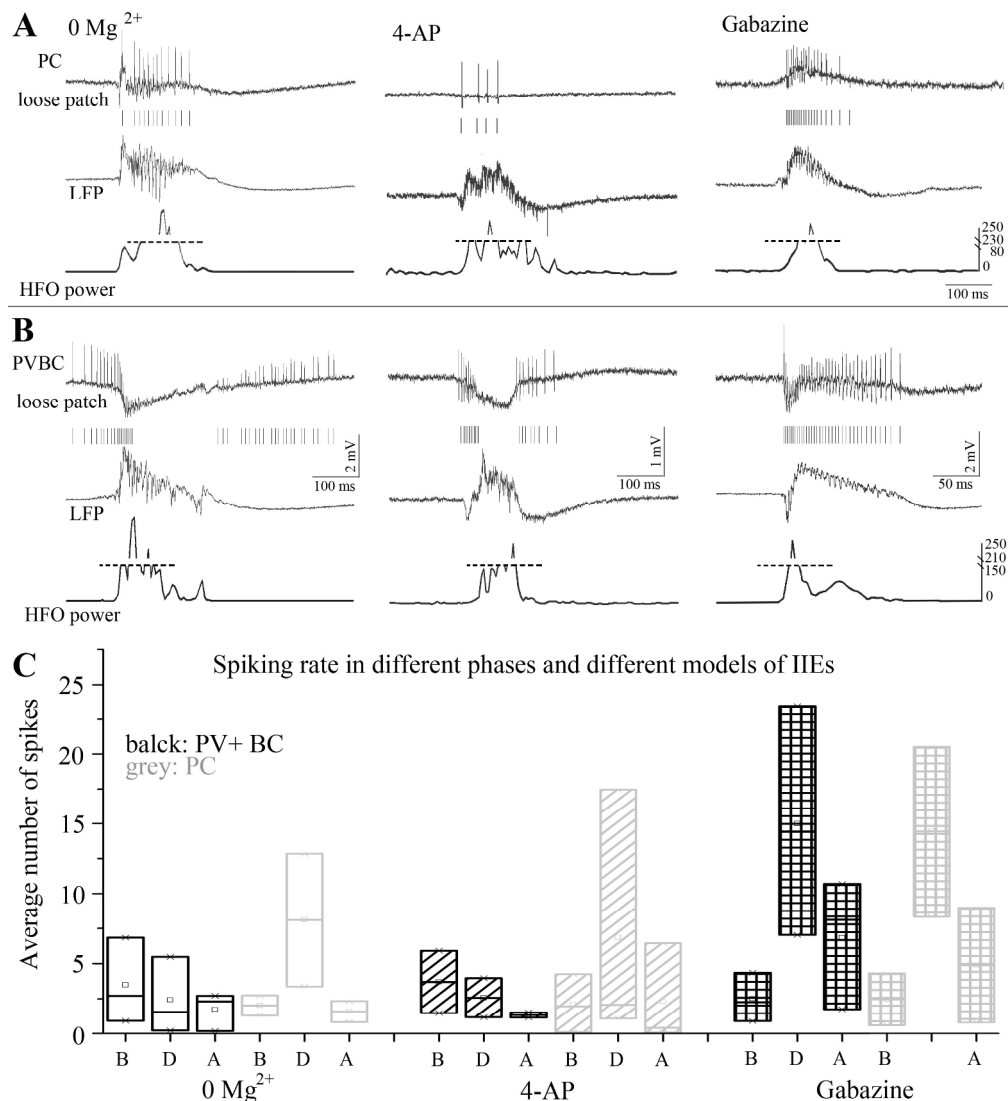


Figure 6: Firing pattern of pyramidal cells and parvalbumin-positive basket cells in other models
 The firing of pyramidal cells (A) and PVBCs (B) was recorded in loose patch mode (upper rows) simultaneously with local field potential recordings (middle rows) in 3 further models of IIEs. The relative power in the 150-400 band (base-normalized to the period before the IIEs) was also calculated and plotted (lower trace) to indicate the period when high frequency oscillation (Boksa et al.) was present in the local field potential. Pyramidal cells mostly fired at (and after) the peak of IIEs. PVBCs cease to fire (similarly to the high K⁺ model) at this stage in the 4-AP and 0 Mg²⁺ models (suggesting they received strong depolarization), but only decrease their spike amplitude in the gabazine model with a continued firing. The high-frequency oscillation in the local field potential coincided with strong pyramidal cell firing in all models.
 C) The firing frequencies in the different models during different phases for the two cell types.

245x274mm (300 x 300 DPI)

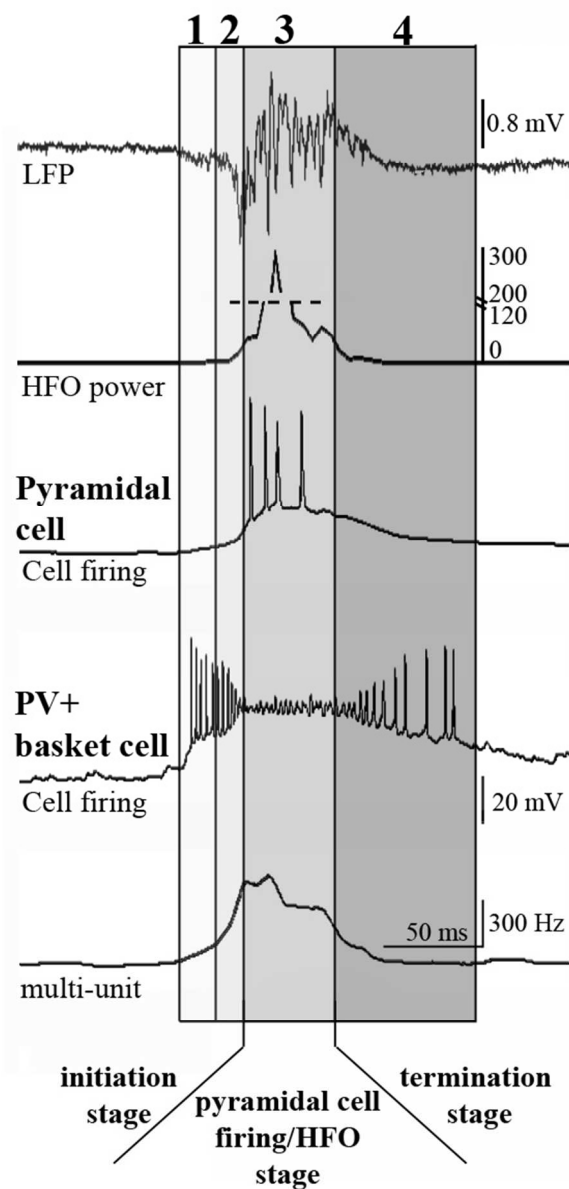


Figure 7: Build-up of depolarization during epileptiform events and its effect on neuronal firing: pyramidal cells start to fire massively when inhibition from parvalbumin-positive basket cells collapses. During the late IIEs we studied, 4 phases can be distinguished: 1. Primary depolarization, PVBCs depolarize and start firing, pyramidal cells start to depolarize, multi-unit activity starts to increase. There is a slow negative deflection in the local field potential. 2. Secondary depolarization, the frequency of PVBC firing further increases while the amplitude drops as the cell depolarizes even further, pyramidal cells depolarize further but do not fire yet, multi-unit activity increases heavily, steep negative drop in local field potential appears. 3. IIE builds up, the power in the 150-400Hz band increases, PVBCs cease to fire (depolarization block) and pyramidal cells start firing as a result of the additional depolarization due to loss of inhibition, multi-unit activity stagnates and starts to drop. A high frequency, large amplitude component (most probably pyramidal cell extracellular spikes, units) appears in the local field potential, accompanied by a positive envelope. 4. The local field potential normalizes, PVBC firing gradually recovers as cells exit the depolarization block, pyramidal cells stop firing and multi-unit activity drops. The figure illustrates the

behaviour of the two cell types in order to compare them; the local field potential was recorded simultaneously with the PVBC, whereas the pyramidal cell was recorded in another experiment. However, in our experiments, pyramidal cells and PVBCs fired during the given phases as illustrated in the figure.

48x98mm (300 x 300 DPI)

For Peer Review

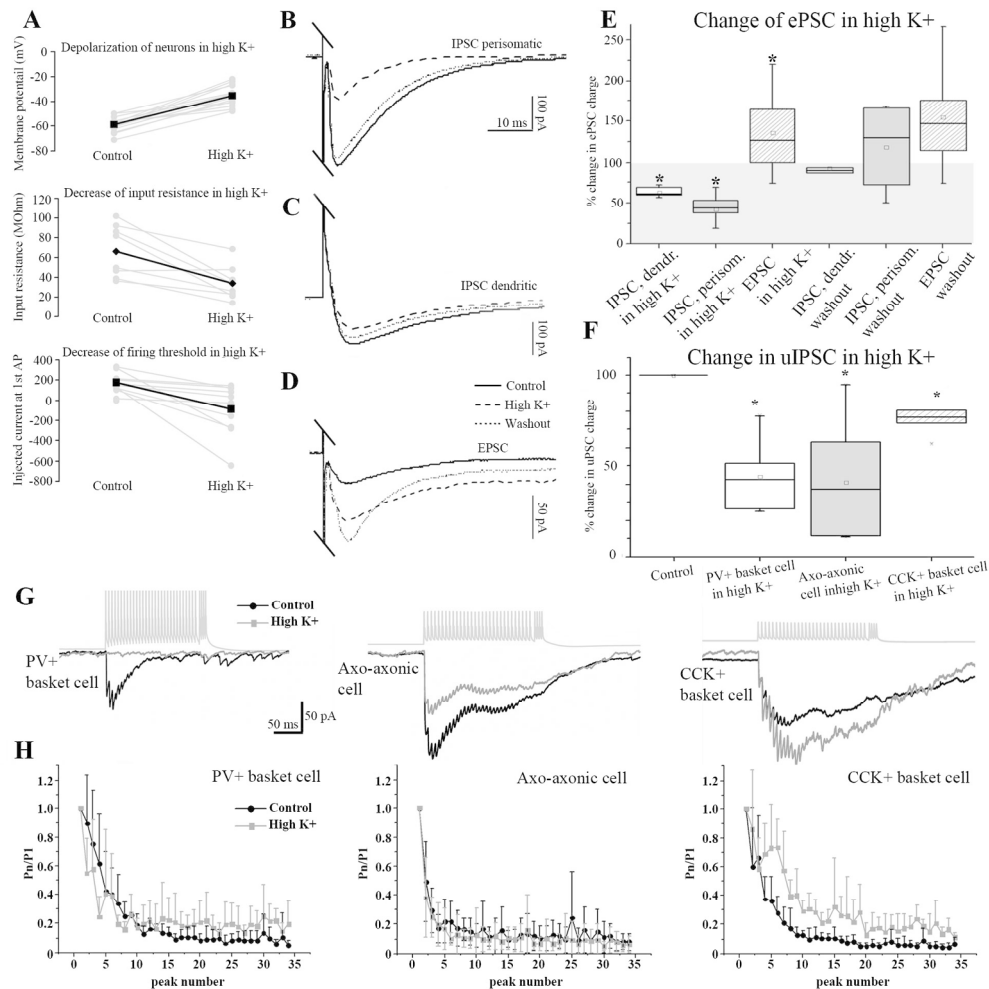


Figure 8: High K⁺ increases excitability, and decreases inhibitory transmission relative to excitatory transmission

A) When the extracellular K⁺ concentration is increased, pyramidal cells become more depolarized (top), input resistance of cells drops to $49 \pm 4\%$ (middle), and excitability increases (bottom), since cells fired the first action potential at a smaller membrane current in high K⁺ compared to control conditions ($n=7$). B-E) shows the increase in the ratio of excitatory to inhibitory transmission in high K⁺. The charge of IPSCs evoked by stimulating perisomatic inhibitory axons (stratum lucidum/pyramidale) dropped after high K⁺ application (B). Similarly, in the case of dendritic IPSCs evoked by stimulating stratum radiatum the charge decreased in high K⁺ (C). However, when EPSCs were evoked in high K⁺ the charge increased (D). E) summarizes the effects on synaptic transmission. F and G) Paired recordings show that inhibitory charge decreases in high K⁺ in the case of PVBCs ($n=7$) and axo-axonic cells ($n=7$), but remains fairly intact in the case of CCK+ basket cells ($n=5$). H) Compared to control conditions (black), short term depression becomes more pronounced in high K⁺ (grey) for the first 10 peaks (afterwards the synapse efficacy drops greatly) for PVBCs, whereas it does not change in the case of axo-axonic cells. In the case of CCK+ basket cells, in high K⁺ the depression was less pronounced. Moreover plasticity could transiently switch from depression to facilitation. Asterisks illustrate significance at $p < 0.05$.

164x163mm (300 x 300 DPI)

Supplemental Results:

Characterization of CCK-DsRed mice

To facilitate the targeting of CCK-positive GABAergic interneurons, a transgenic mouse strain was generated in which DsRed fluorescent protein was specifically expressed in CCK-positive neurons (Mate *et al.*, 2013). In the hippocampus, CCK-positive neurons occur in all layers of the cornu Ammonis. Accordingly, DsRed cells could be found throughout all layers, mostly pyramidale, radiatum and lacunosum-moleculare (**Fig. S1**). In the dentate gyrus, CCK-positive cells are known to be located most frequently at the border between the stratum granulosum and the hilar region, where the DsRed-fluorescent cells were found.

Coexpression of CCK- and DsRed was quantified by combining the intrinsic red fluorescence with green fluorescent immunostaining (Alexa 488) for CCK. In the CA1 and CA3 regions, all layers were involved in the quantification except for str. pyramidale. This was due to the fact that pyramidal cells expressing CCK are extremely dense in these layers, and it is quite difficult to differentiate them from CCK-expressing interneurons. However, our main goal was to characterize the DsRed-expression of CCK-positive GABAergic cells (**Fig. S1**).

A total of 250 cells were quantified and characterized based on their DsRed-expression and CCK suprathreshold immunopositivity, and 85.35% proved to express both DsRed protein and CCK. Details are shown in **Table S1**. In 5.92% of the quantified cells, only DsRed protein was visible, but CCK concentration was below the detection threshold. However, the electrophysiological properties of these cells were similar to that of previously recorded CCK-positive cells. The expression of DsRed fluorescent protein was almost

complete in CCK-immunopositive interneurons; only 8.73% of all quantified cells showed a CCK-immunoreaction without any detectable signal for DsRed protein.

Correspondence of *in vitro* SWR-like events to *in vivo* physiological SWRs

It is an important question to what extent *in vitro* models can reproduce activity patterns recorded *in vivo*. Mere similarity in the amplitude, duration and shape of an activity pattern in field potential recordings from a single layer does not necessarily mean identical generation mechanisms. Therefore, the activity patterns observed in our *in vitro* preparations might be more appropriately named SWR-like activity. However, for the sake of readability we refer to them as SWRs.

Nevertheless, several lines of evidence indicate that the generation mechanisms of these events *in vivo* and *in vitro* are in fact similar. Although SWRs are considered to be generated in the CA3 region and only spread to the CA1 region via the Schaffer collaterals (Buzsaki, 1986), *in vivo* results derive from the CA1 area. Due to the different connectivity of the two regions and the fact that SWRs only propagate to CA1, the generation mechanisms of SWRs in the two areas are most probably somewhat different (e.g., ripple frequency is known to be higher in CA1). Yet *in vivo* SWRs in CA1 (Buzsaki, 1986, Penttonen *et al.*, 1997, Csicsvari *et al.*, 1999, Csicsvari *et al.*, 2000, Buzsaki *et al.*, 2003) and several (though not all) *in vitro* SWR models share important characteristics.

Below we list the features of the SWRs we observed in our slices (see also **Fig. S2, S5** and **Fig. 1** for CSD). For those parameters where *in vivo* data are available from the CA1 area (Buzsaki, 1989, Csicsvari *et al.*, 1998, Csicsvari *et al.*, 2000, Buzsaki *et al.*, 2003, Sullivan *et al.*, 2011), the *in vivo* values are shown in square brackets.

1) SWR episodes occur simultaneously (with a slight delay in CA1) in CA3 and CA1 areas of our slices.

2) The basic parameters of SWR episodes are as follows:

- incidence: 0.86 ± 0.50 Hz (range: 0.02 – 2.04 Hz) [*in vivo*: 0.02 – 3 Hz] (n=82)
- amplitude: 170 ± 196 μ V (range: 14 – 615 μ V; median: 107 μ V; interquartile range: 59 – 225 μ V; n=82)
- duration: 30.4 ± 7.6 ms (range: 16.0 – 53.3 ms) [*in vivo*: 40-100 ms] (n=82).

3) Sharp waves are accompanied by high frequency ripples. In our sample:

- ripple frequency: 186.2 ± 35.0 Hz (range: 109 – 254 Hz) [*in vivo*: 140-200 Hz] (n=66)
- ripple duration: 25.9 ± 13.0 ms (range: 0 – 56.6 ms) [*in vivo*: 25-40 ms] (n=82).

4) SWRs are accompanied by increased unit firing, which is phase-coupled to the negative peaks of the ripple oscillation in str. pyramidale (in our sample, the duration of high spiking activity was 35.9 ± 10.5 ms [*in vivo*: 50-70ms], n=63).

5) The shape of sharp wave field potentials in different hippocampal layers was found to be similar to *in vivo* recordings and resulted in a similar CSD profile (**Fig. 1**, compare to Figs. 1D and 3 from Ylinen et al. (Ylinen *et al.*, 1995), **Fig. S2**).

6) In a recent paper (Hajos *et al.*, 2013), we examined the firing properties of a large set of anatomically identified hippocampal neurons in loose-patch configuration during *in vitro* SWRs in the CA3 region and found that their firing shows similar phase locking to SWRs as identical neuron types examined by Klausberger et al (Klausberger *et al.*, 2003). We note, however, that the latter results are from the CA1 area, but since no such measurements are available so far from CA3, these may be used as a first approximation.

7) We did not use stimulation or any drugs in our baseline conditions; rather, SWRs occurred spontaneously.

Quantification of the evolution of epileptic events

Applying four different epileptogenic methods caused the development of simple EEs followed by more and more complex forms. We aimed to categorize them in order

characterize their features. We are aware that *in vitro* EEs are not necessarily equivalent to human EEG patterns, nevertheless, our identification and classification of EEs was based on characteristics similar to those used in human epileptic patients, as described in the literature (Panzica *et al.*, 1999, Fabo *et al.*, 2008, de Curtis *et al.*, 2012, Fanella *et al.*, 2012). EEs could be categorized as 1: interictal-like events (occurring in all slices and studied in detail later), 2: preictal-like events or 3: ictal-like events, based on their amplitude, duration, structure and incidence (**Fig. 1B**).

1: We defined interictal-like events (IIE) as single, large amplitude 320 μV (220; 520), long duration 140 ms (110; 155) positive field events followed by a negative deflection, and accompanied by high multi-unit activity prior to the rise of the amplitude (the highest multi-unit peak was used for event detection, see *Supplementary Experimental Procedures*). They occurred at an interval of 800 ms (557; 1250). IIEs were seen in most slices (and in all 4 models) producing EEs (high K^+ $n=86$, Gabazine $n=23$, 4-AP $n=8$, 0 Mg^{2+} $n=19$) (**Fig. S3**)

2: The appearance of preictal-like events was preceded by a negative peak (with a robust increase of multi-unit activity), similarly to interictal-like events. However, preictal-like events were immediately followed by 1-5 smaller events with negative deflections, followed by a large positive peak (**Fig. S3**). They appeared less frequently compared to interictal-like events (high K^+ $n=48$, gabazine model $n=14$, 4-AP $n=8$, 0 Mg^{2+} $n=9$), with large amplitude 3300 μV (1187; 4000) and duration 465 ms (335, 793). These events appeared with a recurrence of 1400 ms (637, 7750) due to differences in EE induction.

3: Ictal-like events were seen in a moderate number of slices (mostly in the 0 Mg^{2+} model $n=10$, in the gabazine model $n=5$, and once in the high K^+ model), manifesting as successive large amplitude positive and negative deflections (amplitude: 3500 μV (2200; 4000), duration: 6650 ms (1537; 8000), recurrence: 19000 ms (8200; 25475), where peaks were separated by less than 150 ms and the entire sequence lasted more than 1.5 sec. Field

deflections were always accompanied by an increase in multi-unit activity (2-2.5-fold larger than during SWRs) (**Fig. S3**).

- Description of Epileptiform events in different models

All models lead to a new, highly active network pattern, with similar manifestations. Nevertheless, certain differences were found in this development. For this reason we shall describe briefly the most typical properties of the 0 Mg^{2+} , 4-AP and gabazine models.

The 4-AP model

After adding 30 μM 4-AP to the extracellular solution, SWRs disappeared after 8-10 minutes (duration of transitory phase: 583; 400,642 (median; interquartile range)). In most cases EEs appeared as interictal-like events and further developed to preictal-like events (n=5). In other cases EEs appeared immediately as preictal-like events (n=3). Preictal-like events were the most typical and stable EEs in this model, and did not evolve into ictal-like events. (For the quantification of different event types in different models see **Table S3**).

The 0 Mg^{2+} model

After switching the bath media to one lacking Mg^{2+} it took a relatively long time for the first EE to appear (duration of transitory phase was: 1045; 972,1372 (median; interquartile range)). In some cases mild events (interictal-like events) similar to the most typical event type in the high K^+ model occurred. However, these events proved to be ephemeral, and in most cases they transformed into preictal-like events and later to ictal-like events (n=9). (For the classification of different EE types, see *Supplemental Results/Quantification of the evolution of epileptic events*). In other cases (n=10) there was no gradual build-up seen, EEs appeared either as preictal-like events (n=1) or immediately as ictal-like events (n=9). Ictal-

like events proved to be the most stable event type in the 0 Mg²⁺ model, as they occurred in nearly all experiments (n=17). (Also see **Table S3**)

The gabazine model

When 2 µM gabazine was added to the bathing media SWRs disappeared after few minutes, the time till the first EEs occurred varied greatly among experiments (duration of transitory phase was: 382; 295,896 (median; interquartile range)). The duration of the transitory phase did not correlate in any way to the type(s) of EE that developed later. In some cases (n=9) interictal-like events were the first to manifest and developed into preictal-like events and occasionally further into ictal-like events (n=5). In other cases the first EE type to appear were the preictal-like events (n=14). Interestingly, in these cases ictal-like events appeared, but the morphology of the events proved to be quite conserved throughout the recording. (For the quantification of different event types in different models see **Table S3**)

Morphological identification of biocytin-filled neurons

All recorded neurons were filled with biocytin and visualized with immunofluorescence. Their location and the features of their dendritic and axonal arbours were used to identify them.

-Pyramidal cells had spiny dendrites spanning all layers, and their rarely branching axons were found mainly in stratum oriens and partially in stratum radiatum (PC, n=12, **Fig. 3A**).

-Three types of perisomatic region-targeting interneurons can be found in the hippocampus. We distinguished them by using transgenic mice (expressing eGFP under the control of the parvalbumin promoter or expressing red fluorescent protein under the control of the CCK promoter). The somata of CCK+ basket cells were found in str. oriens or lucidum (CCK+

basket cell, n=5), their dendrites were found in all layers of CA3 (**Fig. S4**). The axon ramified mainly in stratum pyramidale, but some axon collaterals could be observed both in strata lucidum and oriens (**Fig. S4, Fig. 3A**). In PV-eGFP mice, both basket cells (PVBC, n=10) and axo-axonic cells (axo-axonic cell, n=6) express eGFP; therefore, Ankyrin G staining was used to label the axon initial segments of pyramidal cells and to visualize any associations with the biocytin labelled axons (characteristic of axo-axonic cells) (**Fig. S4**). Their dendrites were seen in most layers, and appeared either smooth or occasionally spiny. The axon arbour of both cell types was predominantly present in stratum pyramidale (**Fig. S4, Fig. 3A**), with collaterals in str. oriens and, in the case of PVBCs, in strata lucidum and radiatum. We characterized the firing of all of our recorded cells with a variable current step protocol, and although the majority of PVBCs proved to be fast-spiking and the majority of CCK+ basket cells were regular-spiking, the correspondence was far from perfect (see, (Pawelzik *et al.*, 2002)). Thus, we will use the anatomical terms PVBC and CCK+ basket cell to identify the two cell populations instead of referring to them as fast-spiking basket cells and regular-spiking basket cells.

-Interneurons with axons in the dendritic layers (n=15) were treated as a single group here since their behaviour during EEs was fairly similar. The majority of these cells had their somata either in str. oriens or in str. radiatum, their smooth or spiny, mostly horizontal dendrites in str. oriens or str. radiatum, whereas their axonal arbourisations were widespread in strata oriens and radiatum and occasionally in str. lacunosum-moleculare (presumably OLM cell) or str. pyramidale (presumably trilaminar cell). Some cells had their soma, dendrites and axon collaterals restricted to str. radiatum, rarely penetrating str. lucidum or str. lacunosum-moleculare.

Changes in spike amplitude and half width at increasing K^+ concentration

As we have shown in **Figs. 3, 4 and 5**, the firing pattern of neurons becomes altered during the states that generate epileptiform activity. Even though this change appears to be an important factor in this type of network activity, alterations in the amplitude and half width of action potentials (influencing charge) may influence presynaptic transmitter release.

Therefore, we calculated the spike amplitude and half width at different levels of K^+ by plotting mean values at different time points after washing in increased K^+ (0, 0.5, 1, 2, 5 and 10 minutes). In the case of both pyramidal cells and PVBCs, amplitude and half width gradually increased as a function of time (K^+ concentration) (**Fig. S6**).

While this growth could explain the increased EPSC amplitude and charge recorded in high K^+ (**Fig. 8D**), the same change of interneuron spike parameters cannot be used to explain the drop in inhibitory transmission, and therefore we must conclude that factors other than changes in spike-properties cause the loss of inhibition.

Supplemental Tables:

Table S1. Colocalization of DsRed protein and CCK in hippocampal inhibitory neurons.

	all	% double	% only	% only
CA1, str. Oriens	17	88.24	0.00	11.76
CA1, str. Radiatum	38	78.95	7.89	13.16
CA1, str. lacunosum-	22	77.27	13.64	9.09
CA3, str. oriens	28	71.43	10.71	17.86
CA3, str. lucidum	10	80.00	0.00	20.00
CA3, str. radiatum	54	81.48	14.81	3.70
CA3 str. lacunosum-	16	93.75	6.25	0.00
Hilus	51	82.35	5.88	11.76
DG, str. moleculare	9	100	0.00	0.00
DG, str. granulosum	5	100	0.00	0.00

Table S2: Median number of APs fired at different membrane potentials in CC mode (median and interquartile range is given).

Number of APs	-70	-65	-60	-55	-50	-45	-40	-35	-30
PC	1.7 (0.8; 2.5)	2.4 (0.8; 3.6)	2.9 (0.9; 4.7)	3.3 (0.8; 5.8)	3.8 (1.1; 6.2)	3.9 (1.5; 6.2)	4.2 (2.3; 5.6)	4.7 (3.3; 5.2)	1.6 (1.1; 2.2)
PV+BC	40 (32.2; 9.5)	35.4 (31.3; 36.1)	28.5 (25; 33.2)	25.6 (20.7; 28.3)	20.7 (17.7; 22.9)	14.7 (13; 16)	8.2 (6.6; 15.5)	1.6 (0.4; 15)	0.5 (0; 11.6)
AAC	16.6 (8.3; 19.3)	38.3 (29; 50.6)	29.3 (24.7; 33.2)	20.1 (17.3; 28)	20.7 (19; 22.8)	17.9 (13.4; 19.7)	11.2 (7.9; 15.3)	4.4 (2.4; 10.8)	3 (1.6; 5.7)
CCK+BC	0.8 (0.5; 1.3)	2.5 (1.4; 2.8)	4.2 (2.4; 4.3)	4.1 (2.5; 5)	4.0 (3.2; 5.3)	4.1 (3.9; 6.5)	5.2 (4.3; 6.9)	3 (2; 5.8)	0.2 (0.1; 3.5)
DN	2.2 (1.9; 2.5)	2.1 (2.1; 2.2)	2.5 (2.2; 2.9)	2.9 (2.3; 3.6)	3.0 (2.2; 3.8)	3.1 (2.1; 4)	3.3 (2.2; 4.4)	3.6 (2.3; 4.9)	0.8 (0.6; 0.9)

Table S3: Quantification of different EE types in different models. First number indicates median value, second a third indicate interquartile range (median; Q1, Q3).

	interictal			preictal			ictal		
	duration (ms)	occurrence (ms)	amplitude (μ V)	duration (ms)	occurrence (ms)	amplitude (μ V)	duration (ms)	occurrence (ms)	amplitude (μ V)
high K ⁺	130; 115,150	1250; 1200, 1400	320; 300, 402	315; 305, 348	565; 470, 688	3750; 3400, 4050	1260	990	2200
4-AP	210, 188, 260	750; 595, 1000	217; 213, 245	795, 738, 800	7300; 1300, 13000	1050; 993, 1138			
0 Mg ²⁺	106.5; 95, 111	415, 290, 519	475; 403, 565	855; 838, 873	4550, 3825, 5275	5900; 4850, 6950	8000; 6988, 8225	25300, 22000, 26000	3700; 2225, 5625
gabazine	153; 147, 320	11950; 7670, 15975	800; 775, 875	525; 470, 588	5000; 4000, 15000	2500, 2050, 3400	1298.5; 1179, 1418	6800; 5200, 8400	3250; 3125, 3375

Supplemental Figures:

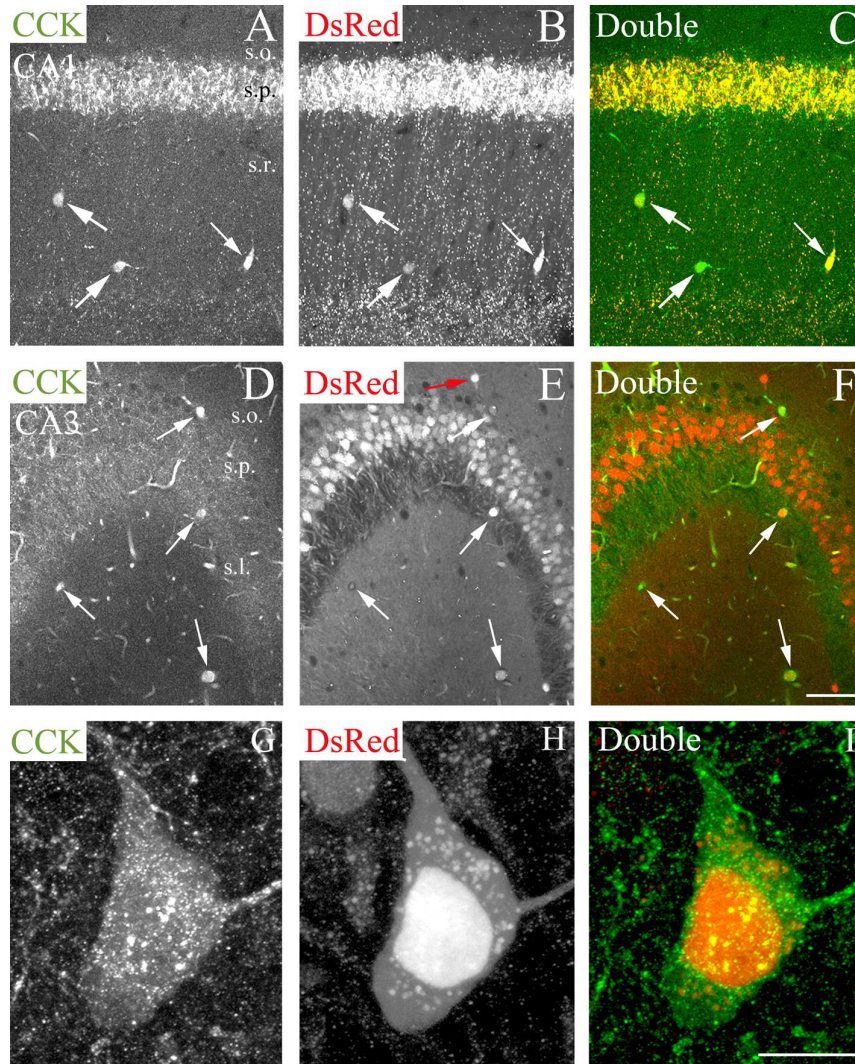


Figure S1: CCK-positivity in DsRed-protein expressing cells

In the CA1 and CA3 regions, most DsRed-positive interneurons are immunopositive for CCK (A-F). Double positive interneurons (white arrows) can be found mostly and very densely in str. pyramidale (since CA1 pyramidal cells express CCK), in radiatum, at the border of strata radiatum and lacunosum-moleculare (A-C) and str. oriens (D-F). Nevertheless, occasionally,

DsRed-expressing cells do not show detectable CCK-positivity (E, red arrow). Higher magnification (G-I) shows that DsRed-positive cells express the protein in their somata and inner membrane compartments (H), whereas CCK-immunoreactions visualize the protein in the cytoplasm (G). Scale: A-F: 50 μm , I: 5 μm .

For Peer Review

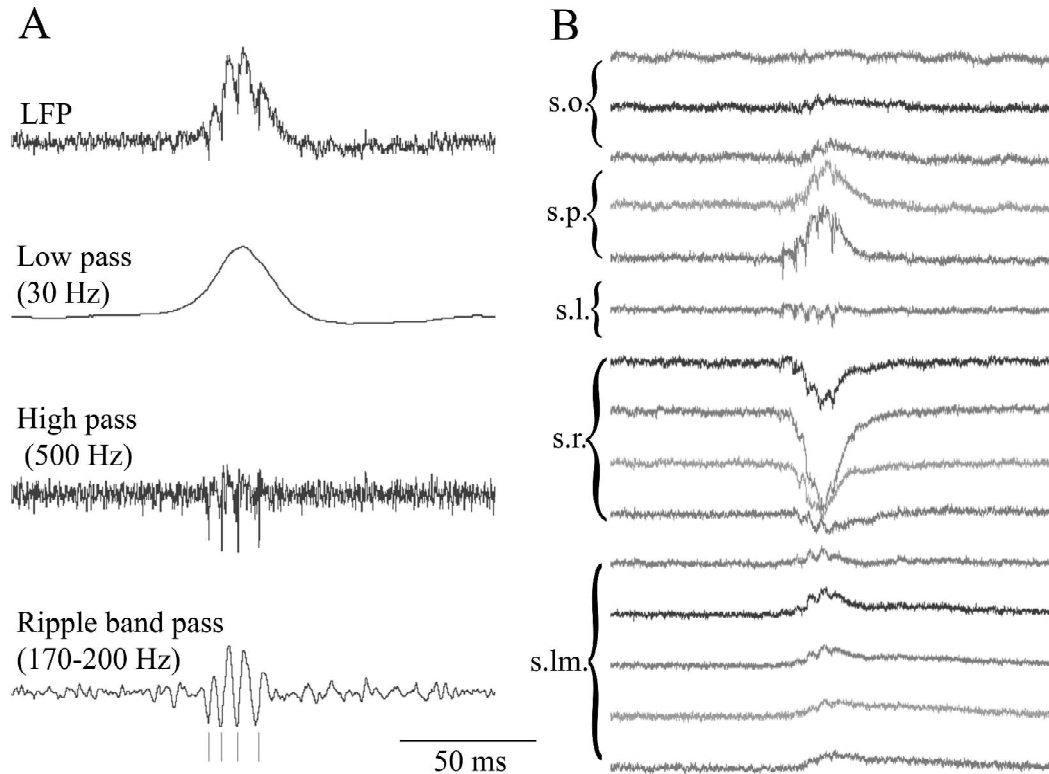


Figure S2: Features of in vitro-recorded SWRs.

A) Components of a SWR demonstrated on unfiltered (upper most) and filtered local field potentials. Low pass filtering (30Hz, second row) shows the sharp wave-ripple envelope and the following negativity without ripples and units. High pass filtering (500Hz, third row) shows the timing of unit activity. The lowest, band-pass-filtered trace shows the ripple activity and the phase-locking of unit spikes (raster lines below) to ripple troughs. B: local field potential recorded with a multi-electrode array shows layer-specific reversals of SWR-related potentials similar to those observed *in vivo*. The CSD created from these recording (shown in Fig 1) also matches the CSD observed *in vivo*.

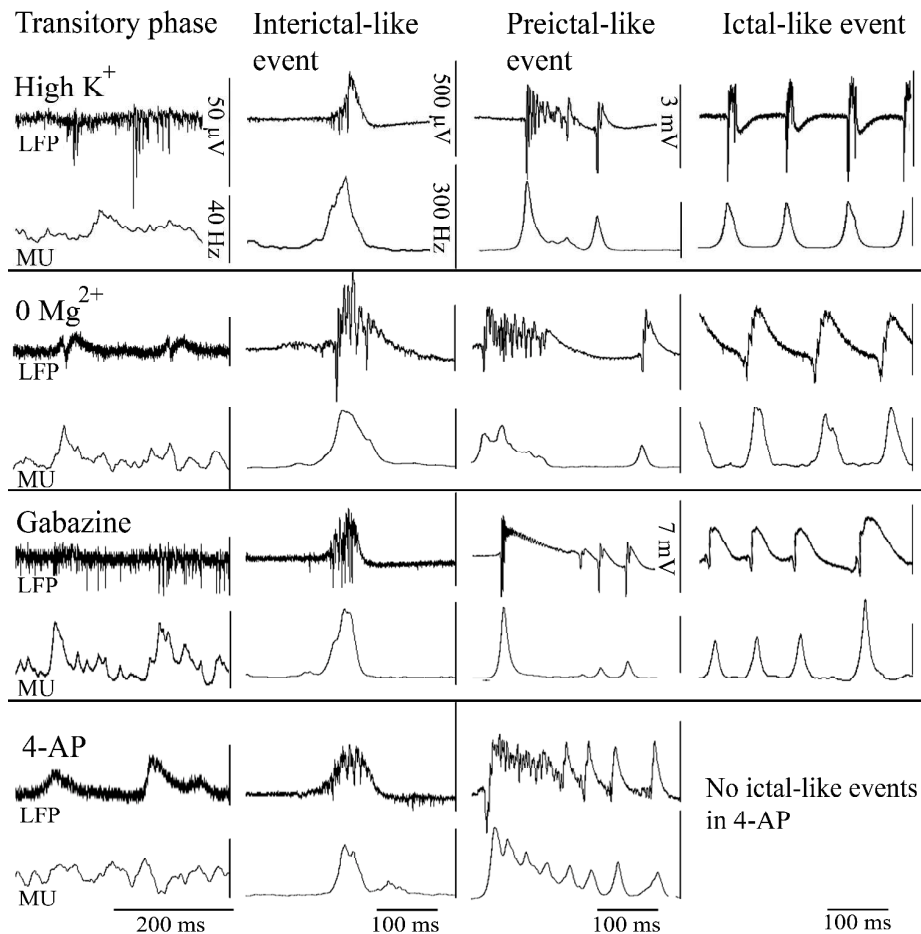


Figure S3: Transition from sharp-wave ripples (SWRs) to epileptiform events (EEs) is similar in 4 different models

EEs can be induced either by elevating extracellular K^+ concentration, omitting Mg^{2+} from the extracellular solution, blocking $GABA_A$ receptor activation, or adding the K^+ channel blocker 4-aminopyridine (4-AP) to the extracellular solution (4 subsequent rows). In all cases, after a transitory period, characterized by low synchrony and high activity (first column), highly synchronous epileptiform events appeared (3 subsequent columns on the right). The amplitude and complexity of EEs could vary among different models; however, phenomenologically similar events occurred with different pharmacological interventions (occurrence of interictal, preictal- and ictal-like activity).

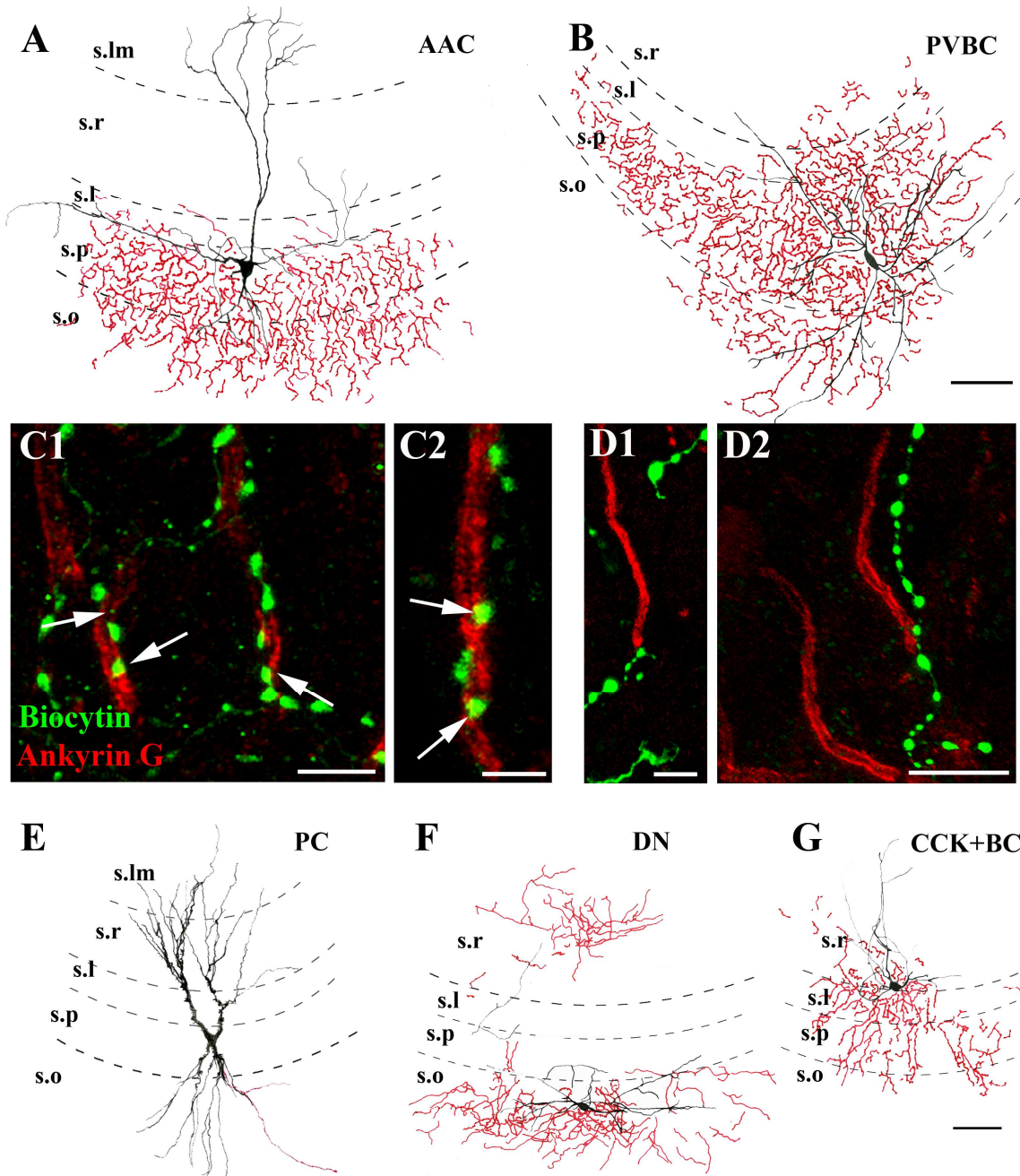


Figure S4: Anatomical identification of CA3 neurons

Camera lucida drawings of the 5 hippocampal neuron types distinguished in CA3.

PV+ axo-axonic cells (A) and basket cells (B) were separated using double-fluorescent staining against ankyrin G (selectively labelling AISs) and biocytin (visualizing the axons of the filled cells). While boutons of the AACs outline the ankyrin G-stained AISs (arrows C1,

C2) of the pyramidal cells, there are no associations between boutons of basket cells and the ankyrin G-stained AISs of the pyramidal cells (D1,D2). Pyramidal cells and dendritic layer-targeting interneurons were distinguished by axonal and dendritic arborisation, whereas CCK+ basket cells innervated the perisomatic region and were immunopositive for CCK and CB1R. Scale: 50 μm

For Peer Review

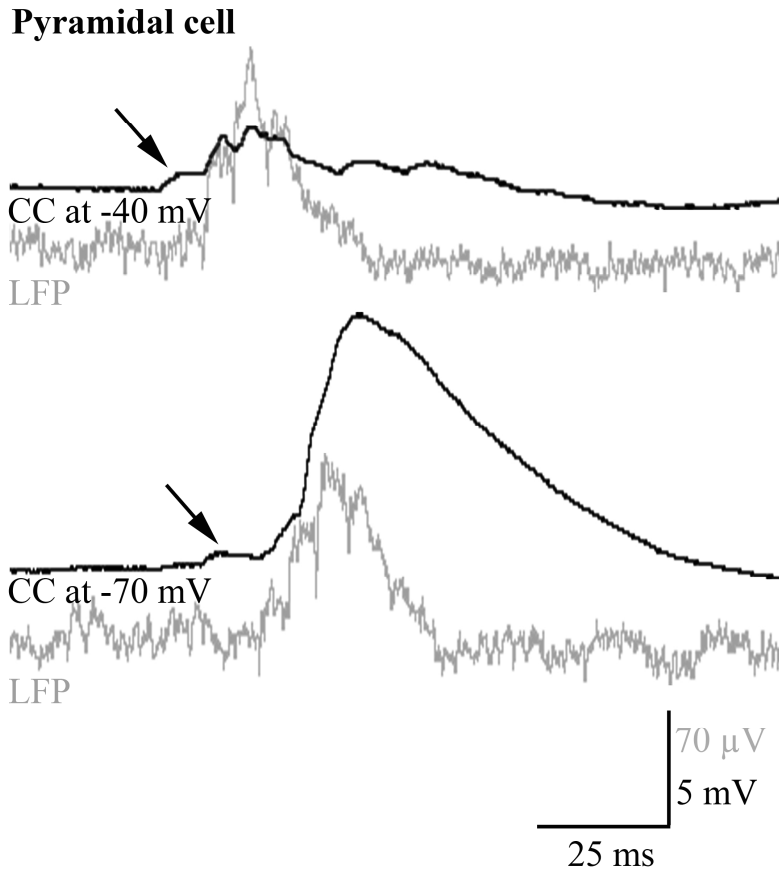


Figure S5: SWRs are preceded by a build-up of depolarizing potentials.

Local field potential from a SWR-producing slice (grey) and intracellular potentials recorded in current clamp mode under control conditions. The pyramidal cell was held at either -70 or -40 mV. At both potentials a depolarization step (arrows) was observed before the local field potential peak, indicating that a build-up of excitation precedes SWRs.

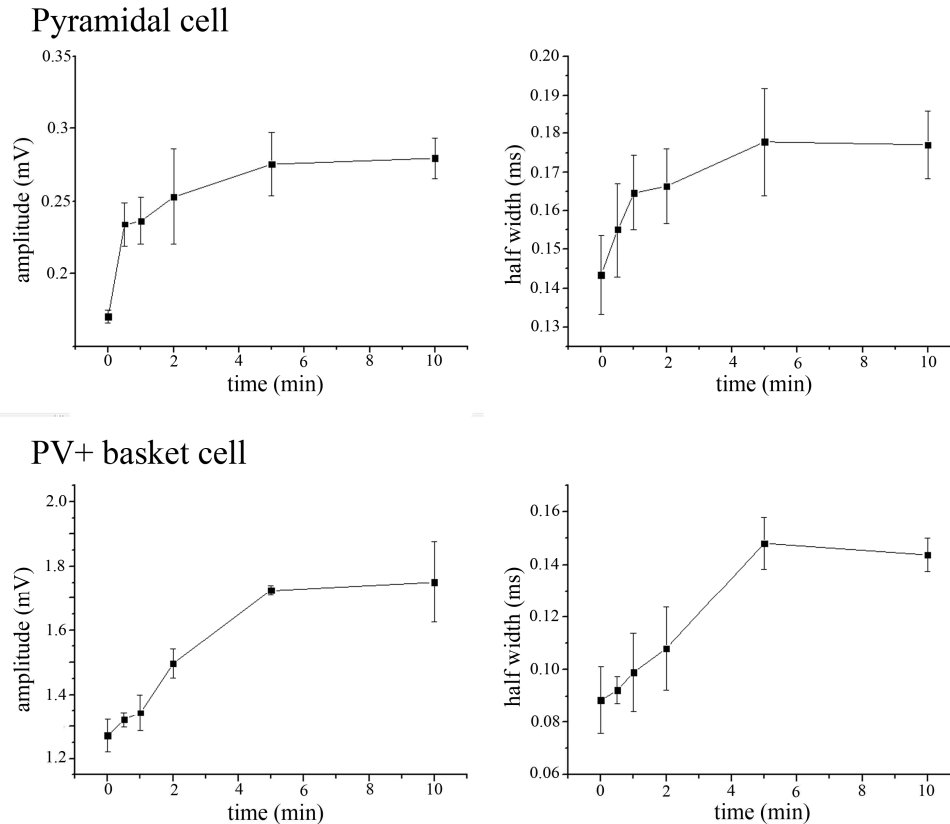


Figure S6: Changes in spike amplitude and half width during the increase of extracellular K^+

Graphs illustrate the increase in cell-attached spike amplitude and half width as a function of time (increase of K^+ concentration). Cells were recorded in loose-patch mode throughout the experiment. In the case of pyramidal cells (and similarly in PVBCs), the rate of increase appeared to be similar for spike amplitude and half width, indicating that the increase in half width appears as a consequence of amplitude growth.

Supplemental Experimental Procedures

Characterization of CCK-DsRed mice

Production of BAC/DsRedT3/CCK transgenic mouse line

BAC engineering technology was used to produce transgenic mice that expressed the T3 variant of the Discosoma red fluorescent protein (Bevis and Glick, 2002) under the control of the CCK promoter and regulation region (DsRedT3/CCK)

v. For more detailed description see Mate et al 2013 (Mate *et al.*, 2013).

Immunofluorescent staining to establish CCK-DsRed colocalization

To quantify the colocalization of DsRed protein and CCK, 3 CCK-DsRed mice were transcardially perfused under equithesine anaesthesia (chlornembutal 0.3 mL/100 g), first with physiological saline (3 min) and then with a fixative containing 0.25% glutaraldehyde (TAAB, UK), 2% paraformaldehyde (TAAB, UK) in a 0.1 M sodium-acetate buffer (pH: 6) for 4 min and finally with another fixative containing 0.25% glutaraldehyde (TAAB, UK), 2% paraformaldehyde (TAAB, UK) in a 0.1 M borate buffer (pH: 8.5). Then, 60 µm thick vibratome sections were cut from the brains, followed by washing in PB. Sections were processed for immunostaining as follows: after being thoroughly washed in TRIS buffered saline (TBS, pH, 7.4) several times, non-specific immunostaining was blocked with 10% normal goat serum (diluted in TBS) for 40 minutes, followed by incubation with a monoclonal mouse antibody against CCK (Cure Antibody lab., UCLA) for 3 days (dilution was 1:2000). For the visualization of the immunopositive elements, Alexa 488-conjugated donkey anti-mouse secondary antibody (Invitrogen, Carlsbad) was used (incubation for 3 hours, dilution was 1:400). Afterwards, sections were thoroughly washed in TBS (3x10 min) and mounted in Vectashield (Vector Laboratories). A minimum of 3 images per layer per region were taken with an A1R confocal laser scanning microscope (Nikon Europe,

Amsterdam, The Netherlands) using a 20× objective. Then DsRed and/or CCK-
immunopositive somata were counted in each micrograph.

Data acquisition and processing

Event detection and analysis.

Signals were filtered with a two-way RC filter to preserve phase. All automatic detection steps were supervised. Spike detection in loose-patch recordings was done on 500 Hz-high-pass-filtered traces using a threshold value of 3 times the standard deviation of the signal. For detecting the frequency of multi-units during recordings, events were detected on a 500 Hz-high-pass-filtered field recording using a threshold value of 1.5 times the standard deviation of the signal, and instantaneous frequency was calculated using a Gaussian kernel with a width of 500ms.

Since a common aspect of EEs was the robust increase of multi-unit activity at the beginning of the event, EEs were detected using this feature. On a 500 Hz-high-pass-filtered field recording, root mean squares were calculated; this way the largest peak represented the largest multi-unit activity and the peak of the EE (IIE). A threshold value of 7 times the standard deviation of the signal was used for event detection. Using this time point as the peak of the event, we measured the duration, the amplitude, and the frequency of occurrence of the IIE on the original trace. The number of spikes were calculated during each IIE and spikes were assigned to three phases of IIEs: spike occurring 100 ms prior the peak (“before” phase), spikes occurring 100 ms following the peak (“during” phase) and spikes occurring from 100 to 200 ms after the peak (“after” phase).

Action potentials during IIEs at different membrane potentials were calculated using the same algorithm, carrying out spike detection in loose patch mode.

Synaptic currents and conductances were calculated by measuring the peak of the postsynaptic current and the area using OriginPro 8.6 software (OriginLab corporation, Northampton, MA, USA).

Quantification of SWR and IIE generation across slices

Slices were categorized into groups 0-3 based on the mean amplitude of SWRs and IIEs as follows: For SWRs, group 0: mean amplitude $<2 \times \text{sd}$ of baseline, group 1: mean amplitude $>2-4.5 \times \text{sd}$ of baseline, group 2: mean amplitude $>4.5-7 \times \text{sd}$ of baseline and group 3: mean amplitude $>7 \times \text{sd}$ of baseline. For IIEs, group 0: mean amplitude $<8 \times \text{sd}$ of baseline, group 1: mean amplitude $>8-10 \times \text{sd}$ of baseline, group 2: mean amplitude $>10-16 \times \text{sd}$ of baseline and group 3: mean amplitude $>16 \times \text{sd}$ of baseline.

Quantification of HFO power

To quantify the HFO component (Figs 3 and 7) an FFT was made on the local field potential and the power content in the 140-400Hz band was summed and plotted against time. It was then normalized to the value of the baseline power in the -200-400msec window before IIEs in the same band. This normalized value was plotted and used to detect the high HFO period. Detection threshold was set to 8 times the standard deviation during baseline period.

Quantification of changes in synchrony.

To quantify changes in the organization of unit firing we defined different measures of fluctuations in the level of instantaneous multi-unit firing. First we detected multi-units using negative threshold crossings of the high-pass-filtered (500Hz) field potential. We then calculated instantaneous frequency of multi-unit firing using a Gaussian kernel with a width of 500 ms. We then normalized this to its low-pass filtered (0.1Hz) version (essentially

instantaneous multiunit frequency divided by the average) to show unit frequency fluctuation without the systematic increase in baseline frequency. We then calculated a time-binned (10sec) standard deviation (sd) of the value and plotted it together with the sd of the low-pass filtered (200Hz) local field potential (**Fig. 2F, bottom**). We also detected local minima and maxima in the normalized frequencies and segmented the recording into short activity bursts by cutting it up into sections containing a maximum and its two flanking minima. The duration, the minimum and maximum values, the total number of spikes and the length of a burst could be calculated and plotted against time. In this way we could detect the duration of activity bursts, but we could not say how focused the activity increase was within the burst. To quantify this, we defined a "burstiness index"; the ratio of maximum frequency difference (between the minimum and maximum frequency) versus the average frequency during the burst. This expressed the relative height (and the narrowness) of the frequency increase during the bursts regardless of the baseline frequency. The burstiness value was again plotted against time (**Fig. 2E**).

There is an issue that should be discussed here. When activity is highly synchronous during the peak of transient high activity events, unit spikes collide and there is no algorithm that can separate them, so multi-units are under-detected and the instantaneous frequency peaks are lower than what is probably expected. However, this does not influence the conclusion of the analysis qualitatively, only quantitatively. The transitional drop in the synchrony of multi-units would be flanked by somewhat higher synchrony values if all spikes were detected.

Anatomical identification of the neurons

The recorded cells were filled with biocytin. After the recording the slices were fixed in 4 % paraformaldehyde in 0.1 M phosphate buffer (PB; pH=7.4) for at least 3 hours,

followed by washout with PB several times. Then sections were blocked with normal goat serum (NGS, 10%) diluted in Tris-buffered saline (TBS), pH 7.4, followed by incubations in Alexa-488 conjugated streptavidin (Molecular Probes, Vienna, Austria, 1:3000). Sections were then mounted on slides in Vectashield (Burlingame, CA, USA). To distinguish basket cells and axo-axonic cells, slices were re-sliced to 40 μm thick sections and processed for immunofluorescence double labelling. Ankyrin G-immunostaining was applied together with biocytin visualization as described above. Staining was carried out as described previously (Gulyas *et al.*, 2010, Szabo *et al.*, 2010). The staining was analysed and z-stacks were taken with a Nikon A1R confocal laser scanning microscope, using a 20x objective (Nikon Europe, Amsterdam, Netherlands). Representative neurons were reconstructed using z-stack maximal intensity projections of each slice (PV+ cell), other cells were reconstructed using a drawing tube (Camera Lucida, Leitz Wetzlar, Germany).

Supplemental References

- Bevis BJ, Glick BS. Rapidly maturing variants of the *Discosoma* red fluorescent protein (DsRed). *Nat Biotechnol.* 2002;20(1):83-7.
- Buzsaki G. Hippocampal sharp waves: their origin and significance. *Brain Res.* 1986;398(2):242-52.
- Buzsaki G. Two-stage model of memory trace formation: a role for "noisy" brain states. *Neuroscience.* 1989;31(3):551-70.
- Buzsaki G, Buhl DL, Harris KD, Csicsvari J, Czeh B, Morozov A. Hippocampal network patterns of activity in the mouse. *Neuroscience.* 2003;116(1):201-11.
- Csicsvari J, Hirase H, Czurko A, Buzsaki G. Reliability and state dependence of pyramidal cell-interneuron synapses in the hippocampus: an ensemble approach in the behaving rat. *Neuron.* 1998;21(1):179-89.
- Csicsvari J, Hirase H, Czurko A, Mamiya A, Buzsaki G. Oscillatory coupling of hippocampal pyramidal cells and interneurons in the behaving Rat. *J Neurosci.* 1999;19(1):274-87.
- Csicsvari J, Hirase H, Mamiya A, Buzsaki G. Ensemble patterns of hippocampal CA3-CA1 neurons during sharp wave-associated population events. *Neuron.* 2000;28(2):585-94.
- de Curtis M, Jefferys JGR, Avoli M. Interictal Epileptiform Discharges in Partial Epilepsy: Complex Neurobiological Mechanisms Based on Experimental and Clinical Evidence. 2012.
- Fabo D, Magloczky Z, Wittner L, Pek A, Eross L, Czirjak S, et al. Properties of in vivo interictal spike generation in the human subiculum. *Brain.* 2008;131(Pt 2):485-99.
- Fanella M, Fattouch J, Casciato S, Lapenta L, Morano A, Egeo G, et al. Ictal epileptic headache as "subtle" symptom in generalized idiopathic epilepsy. *Epilepsia.* 2012;53(4):e67-70.

- Gulyas AI, Szabo GG, Ulbert I, Holderith N, Monyer H, Erdelyi F, et al. Parvalbumin-containing fast-spiking basket cells generate the field potential oscillations induced by cholinergic receptor activation in the hippocampus. *J Neurosci*. 2010;30(45):15134-45.
- Hajos N, Karlocai MR, Nemeth B, Ulbert I, Monyer H, Szabo G, et al. Input-output features of anatomically identified CA3 neurons during hippocampal sharp wave/ripple oscillation in vitro. *The Journal of neuroscience : the official journal of the Society for Neuroscience*. 2013;33(28):11677-91.
- Klausberger T, Magill PJ, Marton LF, Roberts JD, Cobden PM, Buzsaki G, et al. Brain-state- and cell-type-specific firing of hippocampal interneurons in vivo. *Nature*. 2003;421(6925):844-8.
- Mate Z, Poles MZ, Szabo G, Bagyanszki M, Talapka P, Fekete E, et al. Spatiotemporal expression pattern of DsRedT3/CCK gene construct during postnatal development of myenteric plexus in transgenic mice. *Cell Tissue Res*. 2013.
- Panzica F, Franceschetti S, Binelli S, Canafoglia L, Granata T, Avanzini G. Spectral properties of EEG fast activity ictal discharges associated with infantile spasms. *Clin Neurophysiol*. 1999;110(4):593-603.
- Pawelzik H, Hughes DI, Thomson AM. Physiological and morphological diversity of immunocytochemically defined parvalbumin- and cholecystokinin-positive interneurons in CA1 of the adult rat hippocampus. *J Comp Neurol*. 2002;443(4):346-67.
- Penttonen M, Kamondi A, Sik A, Acsady L, Buzsaki G. Feed-forward and feed-back activation of the dentate gyrus in vivo during dentate spikes and sharp wave bursts. *Hippocampus*. 1997;7(4):437-50.
- Sullivan D, Csicsvari J, Mizuseki K, Montgomery S, Diba K, Buzsaki G. Relationships between hippocampal sharp waves, ripples, and fast gamma oscillation: influence of dentate and entorhinal cortical activity. *J Neurosci*. 2011;31(23):8605-16.
- Szabo GG, Holderith N, Gulyas AI, Freund TF, Hajos N. Distinct synaptic properties of perisomatic inhibitory cell types and their different modulation by cholinergic receptor activation in the CA3 region of the mouse hippocampus. *Eur J Neurosci*. 2010;31(12):2234-46.
- Ylinen A, Bragin A, Nadasdy Z, Jando G, Szabo I, Sik A, et al. Sharp wave-associated high-frequency oscillation (200 Hz) in the intact hippocampus: network and intracellular mechanisms. *J Neurosci*. 1995;15(1 Pt 1):30-46.